3

Rheological behaviour of pre-impregnated textile composites

P HARRISON and M CLIFFORD,
University of Nottingham, UK

3.1 Introduction

Virtual design and manufacture of industrial components can provide significant increases in efficiency and reductions of cost in the manufacturing process. This factor provides strong motivation for the composites industry to develop simulation technology for continuous fibre reinforced composites (CFRC) (e.g. Smiley and Pipes 1988; O'Bradaigh and Pipes 1991; de Luca *et al*. 1996, 1998; Pickett *et al*. 1995; McEntee and O'Bradaigh 1998; O'Bradaigh *et al*. 1997; Sutcliffe *et al*. 2002; Lamers *et al*. 2002a,b; Yu *et al*. 2002; Sharma and Sutcliffe 2003). The overriding goal is to make CFRC materials a more attractive option, in a market where composites are often viewed as expensive alternatives to more traditional materials, such as metal and plastic. One of the main challenges in the simulation process is the development of constitutive models that can predict accurately the unique and complex rheological behaviour of viscous CFRC, including textile reinforced thermoplastic composites and thermosetting prepreg composites.

Continuous fibre reinforced composites can be divided into uniaxial CFRC that contain reinforcement in one direction and fabric or textile reinforced composites. The constitutive modelling and associated experimental work on viscous uniaxial and cross-ply CFRC laminates (i.e. laminates consisting of multiple layers of uniaxial CFRC) have received considerable attention over a period of more than a decade. However, until recently, relatively little attention was paid to the characterisation and modelling of viscous textile composites. This situation has changed in recent years; indeed, characterisation and constitutive modelling of viscous textile composites now constitute an active area of research.

The aim of this chapter is to provide the reader with an overview of the current state of rheological modelling of viscous textile composites together with the experimental methods available to characterise their rheology. In section 3.2, a brief discussion of the deformation mechanisms involved in the forming of viscous textile composites is given. Section 3.3 is a review of

the constitutive modelling work for viscous textile composites. The ideal fibre reinforced model (IFRM) is discussed in sections 3.3.1 to 3.3.3. Here the term 'ideal' refers to fibre reinforced incompressible materials that are inextensible along the fibre direction (Hull *et al*. 1994). Attention is drawn to the difficulty in formulating constituent-based predictive models for viscous textile composites using this approach. Attempts to deal with this limitation appear in the literature and these are discussed in sections 3.3.4 and 3.3.6. The inextensibility constraint has been relaxed in some models, as discussed in section 3.3.5. Section 3.4 provides a description and discussion of experimental test methods typically employed in characterising the rheology of viscous textile composites. Finally, section 3.5 describes a visual analysis system used in determining the deformation mechanisms acting during the forming of viscous textile composites over complex shaped components. This technique provides a convenient tool for evaluating the predictions of numerical forming codes.

3.2 Deformation mechanisms

Various deformation mechanisms can occur during forming of a sheet of textile composite material (e.g. Cogswell 1992, 1994; Friedrich *et al*. 1997; Murtagh and Mallon 1997; Mallon and O'Bradaigh 2000). These deformations can be classified according to the length scale over which they occur. Figure 3.1 illustrates various macroscopic deformations. When considering a single layer of textile composite sheet, a single mode of deformation known as *intra-ply shear*, dominates; see Fig. 3.1(a). As will be shown, intra-ply shear is by far the most important and widely studied mechanism in continuum models for textile composites. Intra-ply shear, or trellis deformation, can be visualised by thinking of a woven composite material as a pin-jointed net made from inextensible fibres, with the joints occurring at tow crossover points. As the net is forced to deform, the tows rotate about the crossover points, which results in the material shearing. This is the only mode of deformation considered by the IFRM (see section 3.3), and is also the only mode of deformation modelled by kinematic draping codes (see section 4.2).

Given the relatively high tensile modulus of the reinforcement in, for example, glass or carbon fibre-based textile composites *intra-ply extension*, Fig. 3.1(b), may seem an irrelevant deformation mechanism during forming (i.e. intra-ply shear should offer a much lower energy, and therefore preferable, mode of deformation). However, fibres may extend during forming without excessive forces due to uncrimping of the tows (fibre bundles or yarns) in the textile. Thus, a small degree of intra-ply extension may be expected even in textile composites with high modulus reinforcement. Recent attempts to account for fibre extensibility (and at the same time avoid numerical problems associated with the inextensibility constraint) in finite element (FE) simulations

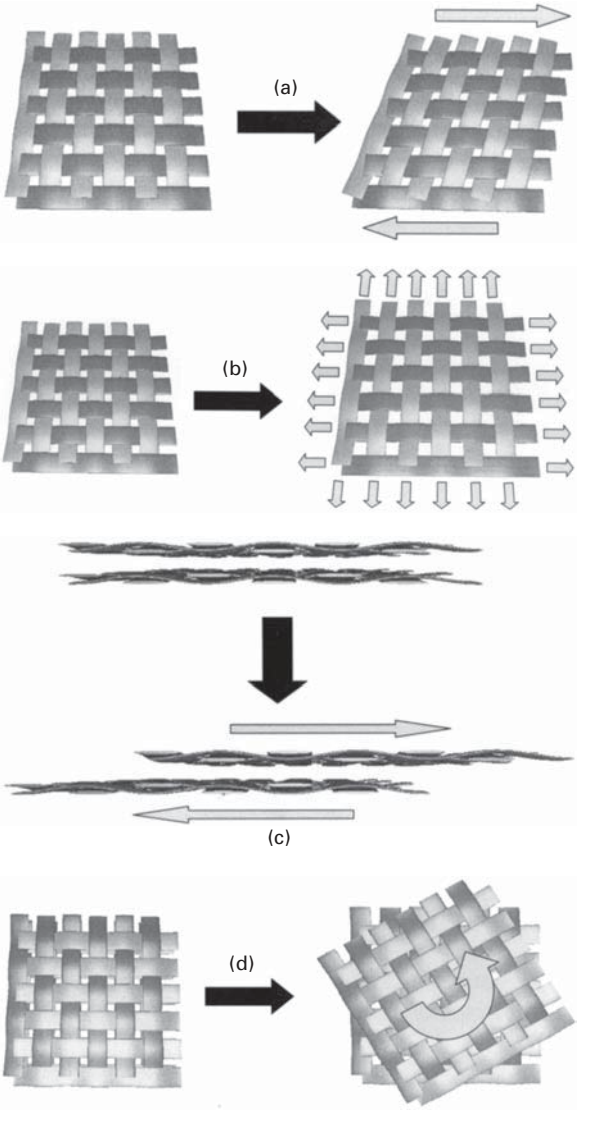

3.1 Macroscopic deformation mechanisms during forming of textile composite material, including (a) intra-ply shear, (b) intra-ply extension, (c) inter-ply slip and (d) inter-ply rotation.

have been made using different approaches (e.g. Lamers *et al*. 2002a; Xue *et al*. 2003; Yu *et al*. 2003) (see section 3.3.6). It is interesting to note that recent interest in self-reinforced polymer–polymer composites (e.g. Prosser *et al*. 2000; Harrison *et al*. 2002d) has made intra-ply extension of even greater relevance, as tows in this type of composite have much lower modulus than for typical woven composites.

For multilayered composites, slip between adjacent layers during forming must also be considered, including *inter-ply slip*, Fig. 3.1(c) and *inter-ply rotation*, Fig. 3.1(d). Inter-ply slip and rotation describe the relative motion of one ply over another as components are formed from multi-ply lay-ups (e.g. Friedrich *et al*. 1997; Murtagh and Mallon 1997; Lamers *et al*. 2003; Phung *et al*. 2003). These modes of deformation are essential if geometries with double curvature are to be formed from multilayer composites without wrinkling, particularly when using plies of initially different orientations.

Recently, homogenisation methods have been used to predict the behaviour of representative volume elements within textiles from consideration of individual tow (fibre bundle) and inter-tow deformations (i.e. mesoscale deformations). Indeed, the potential of textile modelling at the mesoscale has been greatly enhanced recently by increases in computing power and is becoming a growing area of interest for researchers (e.g. Hsiao and Kikuchi 1999; Harrison *et al*. 2004a; Lomov *et al*. 2002; Hagege *et al*. 2003). Examples of mesoscale deformations are shown in Fig. 3.2. Various distinct modes of tow deformation can be identified including *tow-shear*, Fig. 3.2(a), and *tow-squeezing* plus *tow-twisting* (one mode) and *tow-bending* (two modes) about

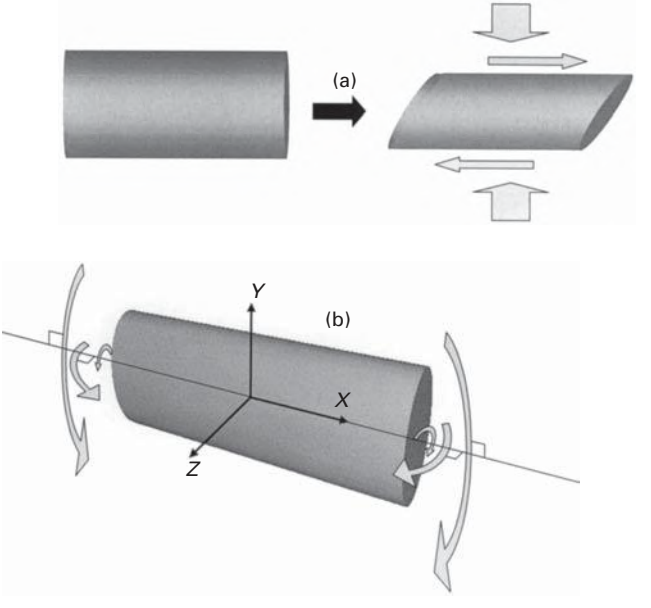

3.2 Mesoscale deformation mechanisms during forming of textile composite material, including (a) tow shear and (b) tow squeezing, twisting and bending. Relative motion between tows can also occur within the ply, including (c) crossover shear and (d) inter-tow shear. Finally, intra-ply slip is another potential deformation mechanism and can be classified as either (e) crossover slip or (f) inter-tow slip.

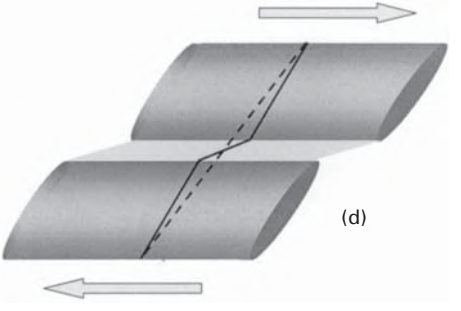

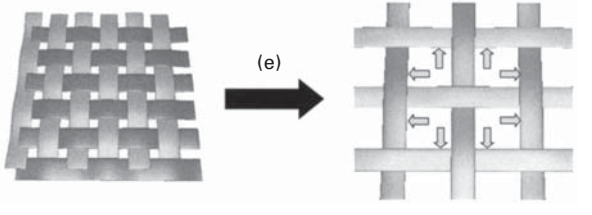

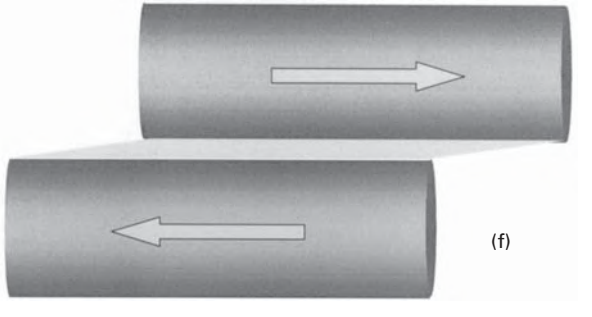

3.2 Continued

the tow axes, Fig. 3.2(b). Mesoscale tow deformations permit macroscale forming of the textile as well as facilitating textile specific deformations such as *mesoscale fibre buckling*. The relative motion of neighbouring tows and their subsequent interaction is also an important factor when modelling textile deformation at the mesoscale. Examples include *crossover shear*, Fig. 3.2(c) (Harrison *et al*. 2002a,b; Zouari *et al*. 2003), which potentially induces large shear strain rates in the matrix fluid between superposed tows, and *inter-tow shear*, Fig. 3.2(d), which arises when the shear rate across tows is less than the average shear rate across the textile composite sheet (see section 3.3.6).

The nature of mesoscale models means that they can include information such as tow architecture, tow and inter-tow kinematics and can also possibly incorporate so-called *intra-ply slip* mechanisms. Two distinct types of intra-ply slip can be identified, *crossover slip*, Fig. 3.2(e) (e.g. Lai and Young 1999), and *inter-tow slip*, Fig. 3.2(f) (Harrison *et al*. 2004b). These mechanisms are a direct result of relative displacements between neighbouring tows and have been observed to play an important role during the deformation of textile composites. Intra-ply slip occurs most readily in loosely woven composites and in some cases can actually improve the formability of the textile (Long *et al*. 2002). However, too much crossover slip can leave resin-rich regions or, in extreme cases, unwanted holes in components as the tows move apart. Crossover slip is important during press forming and hand lay-up, while inter-tow slip is apparent during bias extension tests, Fig. 3.2(f) (Harrison *et al*. 2004b).

Finally, prediction of individual tow properties can be made using knowledge of factors such as matrix rheology and fibre volume fraction, from consideration of micro-scale fibre–fluid interactions within the individual tows. These interactions are illustrated in Fig. 3.3 and include both (a) *intra-tow transverse shear* and (b) *intra-tow axial shear* (see section 3.3.2).

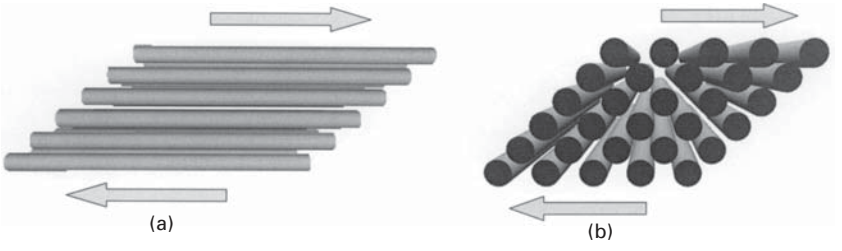

3.3 (a) Shearing the composite parallel to the fibre direction gives a measure of the longitudinal viscosity, η_L. (b) Shearing the composite across or transverse to the fibre direction gives a measure of the transverse viscosity, η_T. Micromechanical models based on these fibre organisations have been developed that relate the matrix viscosity and fibre volume fraction to the two viscosities.

Many of the modelling approaches developed to describe the deformations required to form components have as their goal the elimination of fibre buckling (mainly in relation to uniaxial CFRC) and wrinkles. Although the prediction of these is therefore of prime importance, relatively little work has concentrated on the development and subsequent growth of wrinkles (Hull *et al*. 1991, 1994; Friedrich *et al*. 1997; Li and Gutowski 1997; O'Bradaigh *et al*. 1997; Mander *et al*. 1997; Martin *et al*. 1997b; De Luca *et al*. 1998; Yu *et al*. 2003). The prediction of wrinkles is an important area for future work.

3.3 Review of constitutive modelling work

In this section, a review of the constitutive modelling of viscous textile composites is presented. Examination of the literature reveals various modelling approaches. The first and most widely studied is that of continuum mechanics, in particular models based on the IFRM (section 3.3.1). The IFRM has proved successful in many respects, not least in obtaining analytical solutions to specific well-defined flow deformations. However, certain limitations of the theory have become apparent. These include difficulties found in model-parameter evaluation for 'real' textile composites through experimental characterisation and problems involved in implementing these equations in FE codes.

The review of IFRMs includes work on both viscous uniaxial (section 3.3.2) and biaxial (section 3.3.3) CFRC. While at first sight, the case of the uniaxial IFRM is not directly applicable to textile composites, this work is nevertheless considered for two reasons. The first is to illustrate one of the more ambitious yet desirable goals of CFRC constitutive models, that is, the development of fully predictive models based on properties such as fibre volume fraction and resin viscosity (see also sections 3.3.4 and 3.3.6). Success in this area would dramatically reduce the need for extensive experimental characterisation programmes (section 3.4). The second is because at least one approach to textile deformation modelling, the energy summation method (section 3.3.6), is based on the uniaxial rather than biaxial IFRM.

When implementing a material model in an FE code, an important consideration is the effect of the kinematic constraints of the model on the numerical calculations. The inextensibility constraint of the IFRM leads to arbitrary tensile stresses in the reinforcement directions (see section 3.3.1), stresses that can cause potential problems when calculating force equilibrium. This issue has led certain workers to develop alternative constitutive models for sheet forming predictions (section 3.3.5).

3.3.1 The ideal fibre reinforced model for viscous fluids

The continuum theory of the mechanics of CFRC in a solid or elastic state was developed initially by Spencer and referred to as the elastic ideal fibre reinforced model (Spencer 1972, 1984). This work was adapted by Rogers (1989a) to the case of viscous CFRC through use of the 'correspondence principle' of viscoelasticity. The underlying assumptions of the IFRM for viscous composites have been outlined many times previously (e.g. Hull *et al*. 1994; Rogers 1989a, 1990; Spencer 2000; McGuiness and O'Bradiagh 1998; Mallon and O'Bradaigh 2000) and are repeated here for convenience.

As with the elastic IFRM, two important approximations are used in obtaining solutions in the stress analysis, those of incompressibility and fibre-inextensibility. These conditions can be expressed mathematically as follows. Using $\boldsymbol{D}$, the rate of deformation tensor which can be written in component form as

$$D_{ij} = \frac{1}{2}\left(\frac{\partial v_i}{\partial x_j} + \frac{\partial v_j}{\partial x_i}\right) \tag{3.1}$$

where v_i are the velocity components of a particle at position x_i, the incompressibility condition can be written as

$$D_{ii} = \frac{\partial v_i}{\partial x_i} = 0 \tag{3.2}$$

where the repeated suffix summation convention applies. This first familiar constraint is often used in fluid mechanics. The second constraint of fibre inextensibility is more particular to CFRC theory. The reinforcement fibres are considered as continuously distributed throughout the material and for uniaxial reinforcement are defined at any point by a unit vector, $\boldsymbol{a}(x, t)$ or for textile composites with two directions of reinforcement by $\boldsymbol{a}(x, t)$ and $\boldsymbol{b}(x, t)$. Thus, the inextensibility conditions can be expressed in component form as

$$a_i a_j D_{ij} = a_i a_j \frac{\partial v_i}{\partial x_j} = 0, \qquad b_i b_j D_{ij} = b_i b_j \frac{\partial v_i}{\partial x_j} = 0 \tag{3.3}$$

The fibres convect with the material and so vary in both space and time, hence the material derivative can be used to find the rate of change of $\boldsymbol{a}$ (or $\boldsymbol{b}$):

$$\frac{Da_i}{Dt} = \frac{\partial a_i}{\partial t} + v_j \frac{\partial a_i}{\partial x_j} = (\delta_{ij} - a_i a_j)\, a_k \frac{\partial v_j}{\partial x_k} \tag{3.4}$$

where δ_{ij} is the Kronecker delta. If eqn 3.3 holds then eqn 3.4 reduces to

$$\frac{Da_i}{Dt} = a_k \frac{\partial v_i}{\partial x_k} \tag{3.5}$$

Furthermore, for quasi-static flows, the equilibrium equations

$$\frac{\partial \sigma_{ij}}{\partial t} = 0 \tag{3.6}$$

also hold, where σ_{ij} is the stress tensor. A consequence of these assumptions is that the stress tensor may be decomposed as:

$$\boldsymbol{\sigma} = -p\boldsymbol{I} + T_A\boldsymbol{A} + \boldsymbol{\tau} \tag{3.7}$$

for the uniaxial case with one direction of reinforcement or:

$$\boldsymbol{\sigma} = -p\boldsymbol{I} + T_A\boldsymbol{A} + T_B\boldsymbol{B} + \boldsymbol{\tau} \tag{3.8}$$

for the viscous textile composite with two directions of reinforcement. Here $\boldsymbol{I}$ denotes the unit tensor and $\boldsymbol{A}$ and $\boldsymbol{B}$ are the tensor products:

$$\boldsymbol{A} = \mathbf{a} \otimes \boldsymbol{a}, \boldsymbol{B} = \boldsymbol{b} \otimes \boldsymbol{b}$$

The first two terms appearing on the right-hand side of eqn 3.7 and the first three on the right-hand side of eqn 3.8 are reaction stresses, $-p\boldsymbol{I}$ is an arbitrary hydrostatic term arising from the incompressibility condition and T is an arbitrary tension in the fibre direction arising from the inextensibility constraint. Subscripts A and B indicate the reinforcement direction. $\boldsymbol{\tau}$ is the extra stress tensor. Determining an appropriate form of $\boldsymbol{\tau}$ is the goal of the constitutive modelling using continuum theory.

In the fibre reinforced viscous fluid model the assumption is generally made that $\boldsymbol{\tau}$ depends on both the rate of deformation tensor, $\boldsymbol{D}$, and the fibre reinforcement directions (one direction for uniaxial composites). According to Spencer (2000) $\boldsymbol{\tau}$ must be form invariant with respect to rigid rotations and so has to be an isotropic function of its arguments. The representation of a tensor function of vectors and tensors is an algebraic problem whose solution is known and can be read off from tables (Spencer 1971; Zheng 1994). The eventual form taken by the extra stress tensor depends on numerous factors, such as whether $\boldsymbol{\tau}$ is linear or non-linear with $\boldsymbol{D}$, the number of reinforcement directions in the constitutive model and the presence of material symmetry (Spencer 2000). Various forms of $\boldsymbol{\tau}$ presented in the literature are discussed in sections 3.3.2 and 3.3.3.

However, before discussing these constitutive models, it is useful to provide a brief review of the work done on uniaxial CFRC. In doing so, an important objective in the work on CFRC becomes clear, namely prediction of composite rheology through knowledge of the matrix rheology, the fibre volume fraction of the composite and, in the case of textile composites, the weave architecture. The motivations for such constituent-based predictive modelling are two-fold. Firstly, once the material behaviours of the constituent components are known, then the rheology of any composite comprised of the matrix phase plus continuous inextensible fibres could be predicted, thus allowing the pre-

manufacture optimisation of a composite to suit a potential application. Secondly, characterising the rheological behaviour of, for example, a thermoplastic matrix polymer at different shear rates and temperatures is relatively easy using modern rheometers, compared with the difficult task of characterising a composite material at different shear rates and temperatures (see Section 3.4). Both factors would lead to significant reductions in time and cost in the manufacturing process. For these reasons, much effort has already been made in pursuing predictive models for uniaxial CFRC. The same motivations also apply for textile composites, though as will be seen, the difficulties in producing such a predictive model for textile reinforced viscous composites are greater than for the case of viscous uniaxial CFRC.

3.3.2 Constitutive behaviour of viscous uniaxial CFRC

The rheological modelling of viscous uniaxial CFRC, composites containing fibre reinforcement in just one direction, is closely related to the modelling of viscous textile composites. Rogers (1989a, 1990) was the first to present a three-dimensional linear form for the extra stress tensor for viscous uniaxial CFRC:

$$\boldsymbol{\tau} = 2\eta_T \boldsymbol{D} + 2(\eta_L - \eta_T)(\boldsymbol{AD} + \boldsymbol{DA}) \tag{3.9}$$

A notable feature of this model is the appearance of two constant model parameters, η_L and η_T, which can be related to two distinct material properties; the 'longitudinal' and 'transverse' viscosities of the composite. These two viscosities result from the dynamic interaction between fibre and matrix phases during shear of the composite. This interaction occurs on a microscopic scale and is shown in the schematic of Fig. 3.3. The diagram shows that the composite's transverse viscosity results from individual fibres 'rolling' past one another, while the longitudinal viscosity results from the fibres sliding past one another along their length. Both η_L and η_T are very sensitive to the fibre volume fraction and can be orders of magnitude higher than the matrix viscosity.

Equation (3.9) has been used successfully to perform theoretical investigations of the flow of uniaxial CFRC. Indeed, analytical solutions for the stresses occurring in certain simple forming operations have been suggested as test cases for numerical codes (Rogers 1990; Rogers and O'Neill 1991) and the model has also been applied in producing theoretical analyses of fibre buckling and wrinkling in shear-flows (Hull *et al*. 1991, 1994). However, fundamental to performing any accurate numerical forming simulation for 'real' materials, based on such a constitutive model, is knowledge of the relevant model parameters. Evidently, the question of measuring and perhaps even of predicting the model parameters appearing in eqn 3.9 is crucial. Indeed much work has been performed in pursuing these goals.

Various methods have been devised to measure the two viscosities (Advani *et al*. 1997). Dynamic testing has been conducted using both rotational (Cogswell and Groves 1988; Scobbo and Nakajima 1989; Groves 1989; Groves and Stocks 1991; Cogswell 1992) and linear (Scobbo and Nakajima 1989; Wheeler and Jones 1991; Roberts and Jones 1995) oscillatory experiments. Large strain experiments have also been devised and include steady shear linear 'pull-out' experiments (Goshawk and Jones 1996), squeeze flow experiments (Rogers 1989b; Barnes and Cogswell 1989; Balasubramanyam *et al*. 1989; Jones and Roberts 1991; Wheeler and Jones 1995; Shuler and Advani 1996; Goshawk *et al*. 1997), a vee-bending method (Martin *et al*. 1995, 1997b Mander 1998; Dykes *et al*. 1998) and a picture frame test (McGuiness and O'Bradaigh 1998).

Many of these investigations have been concerned not just with measuring these two viscosities, but also with relating η_T and η_L directly to the matrix viscosity, η_m (Cogswell and Groves 1988; Groves 1989; Scobbo and Nakajima 1989; Balasubramanyam *et al*. 1989; Cogswell 1992; Roberts and Jones 1995; Goshawk and Jones 1996; Shuler and Advani 1996). Indeed, the interest in relating η_L and η_T to η_m has led to the development of analytical models, for example, eqn 3.10 and 3.11 (Christensen 1993) and eqn 3.12 (Coffin *et al*. 1995). Analytical predictions are plotted together with experimental data in Fig. 3.4.

$$\eta_{12} = \left\{ \frac{1 + \alpha(v_f/F)}{\sqrt{[1 - \beta(v_f/F)][1 - (v_f/F)]}} \right\} \eta_m \quad \alpha = 0.8730, \beta = 0.8815 \qquad 3.10$$

$$\eta_{23} = \left\{ \frac{1 + \alpha(v_f/F)}{\sqrt{[1 - \beta(v_f/F)][1 - (v_f/F)]}} \right\}^3 \eta_m \quad \alpha = -0.1930, \beta = 0.5952 \qquad 3.11$$

$$\eta_{12} = \eta_{23} = \left\{ \frac{1}{1 - \sqrt{v_f/F}} \right\} \eta_m \qquad 3.12$$

where v_f is the fibre volume fraction and F is the maximum packing fraction, $F = \pi/4$ for a square array or $F = \pi/(2\sqrt{3})$ for hexagonal array of fibre. Predictions using eqns 3.10–3.12 in Fig. 3.4 are calculated using the maximum packing fraction for a square array of fibres. Other analytical models developed for long discontinuous fibres include those presented by Binding (1991) and Pipes (1992).

Materials tested in the experimental investigations are specified in the legends of Fig. 3.4(a) and (b). APC-2 refers to a thermoplastic composite consisting of carbon fibres (≈ 7 μm diameter) in a poly(etheretherketone) (PEEK) matrix while AS-4 refers to a thermoplastic composite consisting of carbon fibres in a poly(arylenesulphide) (PAS) matrix. Other model materials

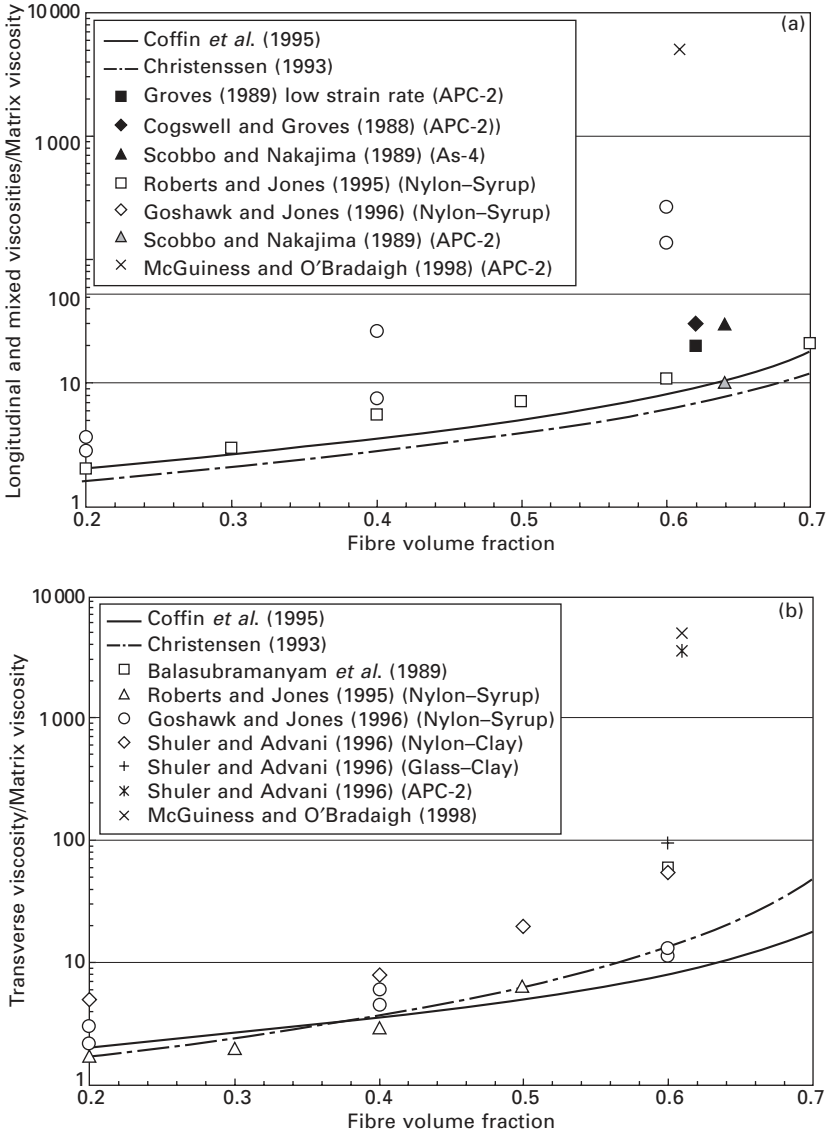

3.4 Data showing ratio between composite and matrix viscosities versus fibre volume fraction from a number of different experimental investigations on uniaxial CFRC. Micromechanical model predictions are also shown. (a) Longitudinal plus mixed mode viscosity measurements and predictions. (b) Transverse viscosity measurements and predictions. The investigation and material are given in the legends.

used in the various investigations include glass (≈ 10–17 μm diameter) or nylon (≈ 210–1000 μm diameter) reinforcing fibres embedded in a matrix of either modelling clay or golden syrup.

Figure 3.4(a) shows longitudinal viscosities plus other apparent viscosities that represent mixed modes of longitudinal and transverse flow induced by rotational rheometers (closed points) while Fig. 3.4(b) shows transverse viscosities. Most experimental data reviewed in Fig. 3.4 revealed a highly non-linear response to shear rate; thus data are subject to the conditions under which they were obtained (e.g. shear strain rate, steady or dynamic data) and are therefore approximate values. Even so, it is clear from Fig. 3.4 that while analytical predictions give a good approximate for a lower limit to the real viscosities of uniaxial composites, these predictions can dramatically underestimate the actual viscosities by an order of magnitude or more. Indeed, viscosities measured on the same thermoplastic composite (APC-2) in different investigations using picture frame, squeeze flow and torsional rheometry testing methods have been reported to vary enormously, by a factor of up to 1000 (McGuiness and O'Bradaigh 1998). Thus, comparison between theoretical predictions and experimental results may well depend on the materials and experimental methods used to collect the data. At present, the reason for the discrepancy between results remains unclear, although this is possibly related to fibre entanglements, non-ideal organisations of fibres, fibre bending rigidity and sample dimensions. A bench-marking exercise, involving several experimental methods and materials, would serve to clarify this ambiguity.

3.3.3 Constitutive models for viscous textile composites based on the IFRM

The initial approach to modelling textile composites, as with uniaxial CFRC, was through the use of the IFRM. However, in this case two fibre directions of reinforcement are incorporated in the assumptions of the continuum theory, as outlined in section 3.3.1. In this section, the biaxial continuum models appearing in the literature are reviewed. Their advantages and disadvantages are discussed before turning attention to methods and models that have been proposed recently as alternatives to the IFRM.

The most general form of the extra stress tensor that is linear with $\boldsymbol{D}$, for a material with two directions of reinforcement, was presented by Spencer (2000)[1]:

[1] An excellent introduction to the continuum mechanical modelling of viscous textile composites.

$$\boldsymbol{\tau} = 2\eta_1\boldsymbol{D} + 2\eta_2(\boldsymbol{AD} + \boldsymbol{DA}) + 2\eta_3(\boldsymbol{BD} + \boldsymbol{DB}) + 2\eta_4(\boldsymbol{CD} + \boldsymbol{DC}^{\mathrm{T}}) + 2\eta_5(\boldsymbol{C}^{\mathrm{T}}\boldsymbol{D} + \boldsymbol{DC}) \quad 3.13$$

where $\boldsymbol{C} = \boldsymbol{a} \otimes \boldsymbol{b}$, $\boldsymbol{C}^{\mathrm{T}} = \boldsymbol{b} \otimes \boldsymbol{a}$ 3.14

and η_1 to η_5 are viscosity parameters of the model. Following Spencer (2000), eqn (3.13) can be simplified by making certain basic assumptions. For example, assuming the two families of fibres are mechanically equivalent, eqn 3.13 reduces to the form

$$\boldsymbol{\tau} = 2\eta_1\boldsymbol{D} + 2\eta_2(\boldsymbol{AD} + \boldsymbol{DA} + \boldsymbol{BD} + \boldsymbol{DB}) + \eta_5\,(\mathrm{tr}\boldsymbol{CD})(\boldsymbol{C} + \boldsymbol{C}^{\mathrm{T}}) \quad 3.15$$

Equivalent forms of eqn 3.12 have been presented previously (Rogers 1989a; Johnson 1995). Equation 3.15 simplifies further by considering the case of a plane sheet, a usual practice when analysing the constitutive equations of uniaxial CFRC and textile composites. Equation 3.15 is of particular interest since numerous attempts have been made to fit this model to experimental data, though none of these comparisons have proved particularly successful (McGuiness *et al*. 1995; Murtagh and Mallon 1995; Canavan *et al*. 1995; Yu *et al.* 2000). Indeed, McGuiness *et al*. (1995) concluded that elastic effects must be included in any successful model, while Yu *et al*. (2000) suggested that no possible combination of the parameters η_1, η_2, η_5 could tune the shape of the predicted curve to match their own experimental data.

For these reasons, various modifications to the linear biaxial continuum model with constant coefficients have since been proposed. The most general non-linear form of the extra stress tensor for an incompressible anisotropic viscous fluid with two directions of inextensible reinforcement was presented by Spencer (2000):

$$\boldsymbol{\tau} = \psi_1\boldsymbol{D} + \psi_2\boldsymbol{D}^2 + \psi_3\,(\boldsymbol{AD} + \boldsymbol{DA}) = \psi_4\,(\boldsymbol{BD} + \boldsymbol{DB}) + \psi_5(\boldsymbol{CD} + \boldsymbol{DC}^T) + \psi_6(\boldsymbol{C}^{\mathrm{T}}\boldsymbol{D} + \boldsymbol{DC}) + \psi_7(\boldsymbol{AD}^2 + \boldsymbol{D}^2\boldsymbol{A}) + \psi_8(\boldsymbol{BD}^2 + \boldsymbol{D}^2\boldsymbol{B}) \quad 3.16$$

where the response functions $\psi_1, \ldots, \psi_8$ are functions of the invariants

$$\mathrm{tr}\boldsymbol{CD},\ \mathrm{tr}\boldsymbol{D}^2,\ \mathrm{tr}\boldsymbol{AD}^2,\ \mathrm{tr}\boldsymbol{BD}^2,\ \mathrm{tr}\boldsymbol{CD}^2,\ \cos 2\phi \quad 3.17$$

where tr represents the trace operation and 2ϕ is the angle between the two fibre reinforcement families.

Equation 3.16 is too complicated to be of practical use without prior consideration of certain simplifying assumptions. Thus, the special case of a plane sheet with power law behaviour was considered and it was suggested that by using this model, the material parameters could be measured by fitting predictions to picture frame data, where experiments are performed at different strain rates. Indeed, in an earlier investigation, McGuiness and O'Bradaigh (1997) proposed isotropic non-linear viscous and viscoelastic

models as well as their equivalent anisotropic counterparts. Two viscosities, η_{12} and η_{33}, with power law behaviours were introduced to represent the resistance to in-plane and through thickness deformations and a Kelvin model (spring and dashpot in parallel) was used to introduce viscoelasticity, as recommended by Canavan *et al*. (1995). Models proposed by McGuiness and O'Bradaigh (1997) are summarised by Mallon and O'Bradaigh (2000). Comparisons between experimental data produced by the picture frame experiment (see section 3.4) and model predictions were presented. The most appropriate choice of constitutive model was found to depend on the particular material under investigation. Thus, McGuiness and O'Bradiagh (1997) were able to demonstrate how picture frame tests can be used to characterise the rheological response of a given textile composite in terms of non-linear rheological models. However, the main drawback with this approach is the large number of experiments required to fit the model parameters.

Another notable success of the continuum approach has been its capacity to predict the asymmetric stress response to shear in opposite directions of certain textile architectures, through consideration of fabric symmetries (Spencer 2000). This unexpected stress response was measured experimentally in picture frame tests (Canavan *et al*. 1995; McGuinness and O'Bradaigh 1997).

The most recent modification to biaxial continuum models incorporating the inextensibility constraint has been to include plastic yield behaviour (Yu *et al*. 2000; Spencer 2002). Yu *et al*. (2000) use a modified version of eqn 3.15 by including an equivalent von Mises yield criteria in the model and compared the model with experimental data. Spencer (2002) described a more general model including both plastic and non-linear behaviour though, as yet, the model remains untested against experimental data.

It should be noted that there is an important difference between these biaxial constitutive models and those applicable to uniaxial CRFC (see section 3.3.2). That is, for uniaxial CFRC the viscosity parameters, for example in eqn 3.12, can be related directly to simple micro-mechanical shearing mechanisms (see Fig. 3.3). However, while the viscosity parameters in eqns 3.13, 3.15 and 3.16 may be related indirectly to these micro-mechanics (Spencer 2000) a simple relationship between biaxial-model viscosity parameters and micro-mechanical mechanisms no longer exists. For this reason, the development of simple micro-mechanical models, which predict the relationship between the matrix viscosity, η_m, and the model parameters appearing in these equations is impossible. Since determination of the parameters in the various biaxial constitutive models requires a considerable amount of experimental work, especially if various temperatures are to be considered, the need for constituent-based predictive models is just as important for modelling textile composites as for modelling uniaxial CFRC. Thus, alternative modelling techniques are now being employed to meet this end (see sections 3.3.4 and 3.3.6).

Finally, as was noted in the introduction, the strong constraints inherent in the IFRM have been found to cause problems when attempting to implement this model in numerical codes. Thus, while the IFRM is useful in providing analytical solutions to specific simple flow problems, relaxation of these constraints is often required when implementing constitutive models in FE software. This point has played a significant role in the development of some of the more recent constitutive models that are suitable for implementation in FE codes.

3.3.4 Predictive models for viscous textile composites based on homogenisation methods

The homogenisation technique can be applied to periodic materials and consequently has proved useful in modelling the deformation stresses (and thermal properties) of textile composites (Hsiao and Kikuchi 1999; Peng and Cao 2002). The method involves modelling the composite using FE analysis on various length scales and using the smaller length scale models to predict the material properties at a larger length scale. Results from the larger-scale predictions can then be fed back into the smaller scale and the process is repeated. Thus, use of the homogenisation method facilitates forming predictions based on fibre angle, volume fraction and properties of the constituent materials in the textile composite (Hsiao and Kikuchi 1999). The method potentially solves one of the main limitations of the biaxial IFRM, i.e. the need for expensive and time-consuming characterisation experiments required to fit model viscosity parameters. A second problem associated with the IFRM, namely numerical problems caused by the fibre inextensibility constraint, was tackled by use of a numerical penalty method. However, the homogenisation method does have its drawbacks, including the difficulty in producing FE meshes of the potentially complicated weave-architectures, the associated large amount of computational power required to run these simulations and the difficulty involved in implementing such a model in commercially available FE codes owing to the lack of an explicitly written constitutive equation.

3.3.5 Explicit constitutive models for viscous textile composites with fibre extensibility

As with the IFRM this family of constitutive models is expressible in explicit matrix form; however, the models differ in that they avoid the strong constraint of fibre inextensibility. Indeed a main aim here has been to develop models that are easy to implement in commercial FE codes. Different approaches have been employed, including the development of entirely new non-orthogonal constitutive models (Xue *et al*. 2003; Yu *et al*. 2002, 2003) as well as direct

modification of the IFRM (Lamers *et al*. 2002a,b, 2003). The model of Yu *et al*. (2002) was developed through consideration of stresses induced in a conceptualised pin-jointed net structure consisting of non-orthogonal tows of given tensile modulus. The resulting constitutive equation was formulated by calculating linear elastic stresses induced in the non-orthogonal net structure by a superposition of imposed tensile and simple shear strains. Consequently, the equation is valid for small axial strain deformations along the reinforcement directions. However, the incremental form of the equation means that it can be implemented in numerical codes and used to model large strain behaviour. Use of the non-orthogonal reference frame allows the shear behaviour measured in picture frame tests to be incorporated directly into the model.

In another non-orthogonal model (Xue *et al*. 2003) material tensile properties were determined through tests on textiles with orthogonal tows, i.e. before shear (Boisse *et al*. 2001), while shear properties were determined from picture frame tests (see section 3.4). The stress tensor is expressed in the 2D non-orthogonal reference frame using these properties and then transformed to the global Cartesian frame for use in FE calculations. The resulting model is valid for large strains. Finally, another approach has been simply to relax the strong constraints of fibre inextensibility and incompressibility to produce a modified IFRM (Lamers *et al*. 2002a,b, 2003). At present the main drawback of these explicit models is that, as with the IFRM, a large amount of characterisation experiments are required to fit the material parameters. Indeed, this problem is exacerbated for some of the latest non-orthogonal models since these have been developed for rate-independent mechanics, i.e. shear force is characterised by an elastic rather than viscous material response. A potential solution to this problem is to fit these explicit models to shear force versus shear angle curves predicted using energy summation methods (see section 3.3.6). Further information regarding the implementation of explicit models in FE software can be found in Chapter 4.

3.3.6 Shear force prediction for viscous textile composites based on energy summation

A predictive method of calculating the shear force versus shear angle behaviour of textile composites has been proposed based on energy summation. The main inputs of the model are the fibre volume fraction and viscosity of the viscous matrix (Harrison *et al*. 2002a,b, 2003). The method is based on a combination of simple models that are used to calculate the energy dissipation of various micro- and mesoscale deformations. Deformation of the tows is modelled using uniaxial continuum theory (Rogers 1989a) plus associated transverse and longitudinal viscosity micro-mechanical models (e.g. Christensen 1993; Coffin *et al*. 1995). In addition, mesoscale observations of inter-tow shear within the textile composite have resulted in the development

of a simple 'crossover shear' model (see Fig. 3.2d). This model is based on observations of heterogeneous shear strain within the textile (see Fig. 3.5a) (Harrison 2002a; Potter 2002), which results in the relative rotation of superposed tows. Note that a homogeneous shear across the textile would imply that tows within the textile should shear at the same rate as the average shear rate across the textile. If this were the case then the white lines marked on the textile, shown in Fig. 3.5a, would be continuous rather than broken. This would imply zero relative velocity and hence zero shearing of the matrix fluid between the crossovers.

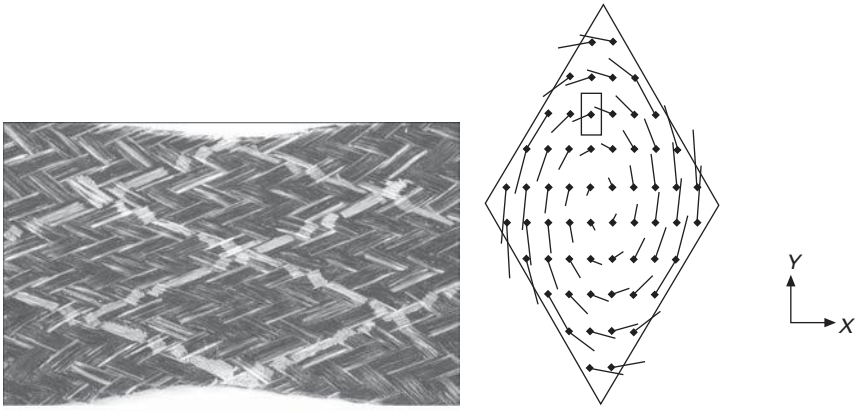

3.5 (a) Example of discontinuous shear strain profiles across various textile materials. The broken form of initially continuous lines drawn on the 2 × 2 twill weave glass/polypropylene thermoplastic composite, sheared in a bias extension test at 180 °C, serves to illustrate the in-plane strain profile. (b) Relative velocity field beneath a single tow crossover where velocities are indicated by vector lines. A rectangular element is drawn around one of the points in order to discretise the crossover area for energy calculations. In this example, the tow shear strain rate $\dot{\gamma}_t = \dot{\theta}/2$ and the shear angle $\theta = 30°$.

Incorporation of the observed mesoscale kinematics (i.e. heterogeneous shear) has two important effects. Firstly, modified versions of the homogeneous rate of deformation tensor must be used for both tow and inter-tow regions. Secondly, a relative velocity exists between the two sets of reinforcement tows at the tow crossovers thus energy dissipation in this region must be considered (see Fig. 3.5b).

The advantage in this method is the low computational power required to make shear force versus shear angle predictions, making it a fast, efficient method of producing first estimates of the material behaviour as a function of shear rate, shear angle and temperature. Example results from the energy

model are compared against normalised experimental bias extension (see section 3.4.2) measurements in Fig. 3.6 (from Harrison *et al.* 2003). The normalisation procedure is described in section 3.4.3. Experiments were performed on a pre-consolidated glass/polypropylene 2 × 2 twill weave thermoplastic composite at 165 and 180 °C. Valid experimental data for high shear angles are impossible to obtain using the bias extension test. However, picture frame tests (see section 3.4.1) can produce this data and have corroborated the sharp increase in shear force predicted by the model. Inputs into the energy model included matrix shear rheology, fibre volume fraction, observed tow kinematics and weave architecture. Future work is still required in order to predict tow kinematics during forming.

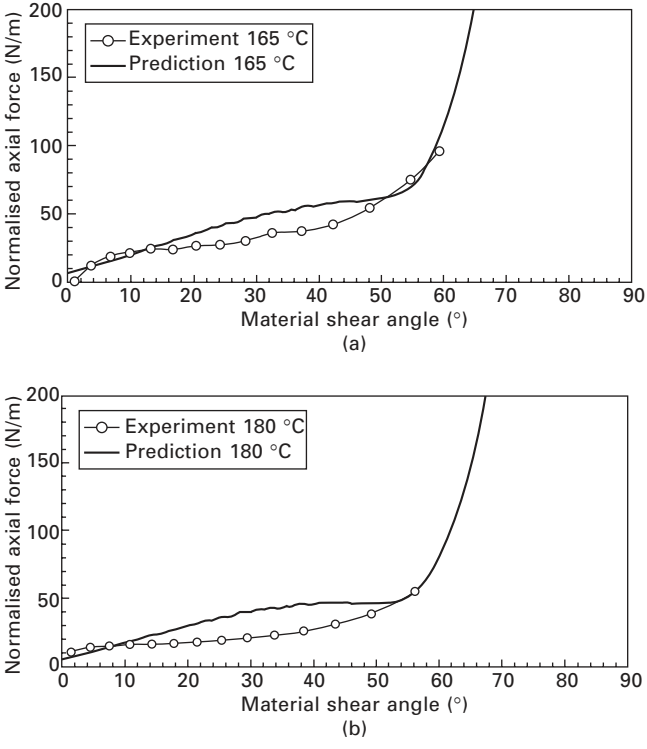

3.6 Bias extension test results together with theoretical predictions. Experiments were performed on a pre-consolidated glass/polypropylene 2 × 2 twill weave thermoplastic composite at (a) 165 °C and (b) 180 °C.

Since energy calculations produce force versus shear angle curves rather than predicting stresses within the material, this energy summation approach is not strictly speaking a constitutive model. However, results can be used to

fit parameters of the constitutive models described in sections 3.3.3 and 3.3.5. In so doing, far less picture frame and bias extension experiments would be required and their intended purpose would be model evaluation rather than characterisation and parameter fitting.

3.4 Characterisation methods

Various experimental methods for characterising the rheology of woven impregnated CFRC have been proposed. Experimental data from such tests can play two important roles; either in fitting the parameters of constitutive models derived from continuum mechanical assumptions, or else in evaluating the accuracy of constitutive models based on a constituent-based predictive approach. The characterisation of textile composites using rotational rheometers was suggested originally by Rogers (1989a), though more specialised test methods have since been developed. Two test methods in particular have seen widespread application, namely the picture frame test (McGuiness *et al*. 1995; Canavan *et al*. 1995; Long *et al*. 1997; McGuiness and O'Bradaigh 1997, 1998; Harrison *et al*. 2002a; Wilks *et al*. 1999; Mallon and O'Bradaigh 2000; Lussier *et al*. 2002; Lussier and Chen 2000; Lebrun *et al*. 2003; Milani *et al*. 2003) and the bias extension test (Yu *et al*. 2002; Murtagh and Mallon 1995; Lebrun and Denault 2000; Lebrun *et al*. 2003; Milani *et al*. 2003; Harrison *et al*. 2003). As industry makes greater use of manufacturing design tools such as finite element simulations, the need to standardise these test procedures is urgent. Work in this direction has been conducted recently (Blanchard *et al*. 2001; Lebrun *et al*. 2003; Harrison *et al*. 2004b; Peng *et al*. 2004).

3.4.1 Picture frame test

The picture frame (or rhombus) test has been used to measure the force generated by shearing technical textiles and textile composites. A sample of fabric is held in a 'picture frame' hinged at each corner (see Fig. 3.7). The frame is loaded into a tensile test machine, and two diagonally opposite corners are extended, imparting pure, uniform shear in the test specimen on a macroscopic scale. There is no uniformly applied standard test procedure, and individual researchers have modified the test method to improve the repeatability and accuracy of test data. One point requiring particular attention is the restraining technique used to hold the sample in the picture frame (McGuiness and O'Bradaigh 1998). Some researchers prefer to constrain the ends of the fabric using pins and a very low clamping force to avoid fibre tensile strain and excessive bending of tows (Harrison *et al*. 2003). Others prefer to prevent fibres from slipping, by tightly clamping the edges of the test specimens under a clamping plate (Milani *et al*. 2003).

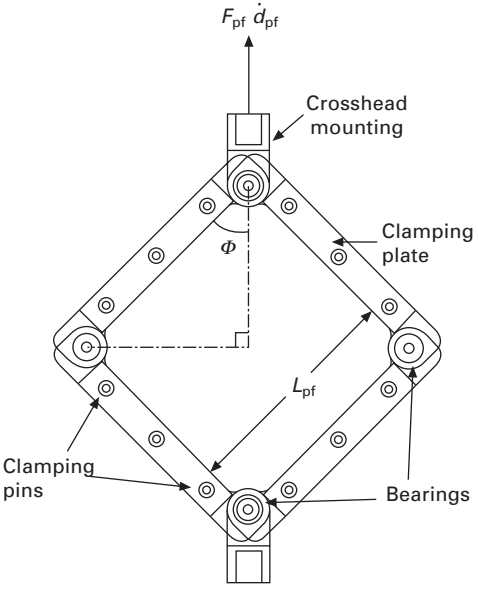

3.7 Picture frame shear rig. L_{pf} is the side length measured from the centre of the hinges, F_{pf} is the axial force measured by the crosshead mounting, d_{pf} is the rate of displacement of the crosshead mounting and the material shear angle, θ, is defined as $\pi/2 - 2\Phi$.

Recently a method of reducing error due to fibre tensile strain through the use of sample 'tabs' has been suggested (Lebrun *et al*. 2003). The choice of restraining method is made according to the variability of the experimental data, which depends on the type of material under investigation. The axial force required to pull the crosshead of the testing machine is recorded and the shear force can be calculated subsequently using:

$$F_s = \frac{F_{pf}}{2\cos\Phi} \qquad 3.18$$

where Φ is the frame angle and F_{pf} is the measured axial picture frame force. Test data are often analysed to produce graphs of shear force against shear angle, where the shear angle is defined as:

$$\theta = \pi/2 - 2\Phi \qquad 3.19$$

Alternatively, axial force can be plotted rather than the shear force to facilitate comparison of the data with bias extension results, which are not necessarily the result of pure shear (see section 3.2). Consideration of the geometry of the test shows that θ can be related directly to the displacement of the crosshead, d_{pf}, by

$$\theta = \frac{\pi}{2} - 2\cos^{-1}\left[\frac{1}{\sqrt{2}} + \frac{d_{pf}}{2L_{pf}}\right] \quad 3.20$$

where L_{pf} is the side length of the picture frame, i.e. the distance between centres of the picture frame bearings and d_{pf} is the displacement of the crosshead mounting (see Fig. 3.7).

The picture frame test procedure is simple to perform and results are reasonably repeatable. Since the deformation of the material is essentially homogeneous throughout the deforming sample (edge effects being ignored), the kinematics of the material deformation are readily calculated, facilitating rheological analysis of the results (McGuiness and O'Bradaigh 1997). A major benefit of the test is that the shear angle and current angular shear rate can be related directly to the crosshead displacement and displacement rate. However, one of the main concerns with the test is the boundary condition imposed on the sample. Loose pinning of the sample edges in the side clamps may fail to induce the required kinematics, whereas tight clamping of the sample edges can cause spurious results if the sample is even slightly misaligned. Another concern with the boundary conditions of the picture frame test is related to the influence of the metal rig on the temperature profile across the sample. During the high-temperature testing required for thermoplastic composites, the rig has been shown to cool the material immediately adjacent to the deforming sample, which may influence results significantly (see section 3.4.3).

Normalised results (shear force divided by side length of picture frame, L_{pf}) from picture frame experiments conducted at room temperature at three constant angular shear rates, 0.93, 4.65 and 9.3° s^{-1}, on a 5-harness satin weave carbon–epoxy prepreg are shown in Fig. 3.8. The issues regarding normalisation of shear data from characterisation experiments are discussed in section 3.4.3. Each curve is an average of four tests. The data show a non-linear increase in shear force with increasing shear rate, indicative of a shear-thinning viscous material response.

3.4.2 Bias extension test

The bias extension test involves clamping a rectangular piece of woven material such that the warp and weft directions of the tows are orientated initially at ±45° to the direction of the applied tensile force. The material sample can be characterised by the length/width ratio, $\lambda = L_o/w_o$, where the total length of the material sample, L_o, must be at least twice the width, w_o. The reason for this can be seen when analysing the idealised deformation of a material sample in a bias extension test.

Figure 3.9 shows an idealised bias extension test sample with $\lambda = 2$, in which the material is divided into three regions. If the tows within the sample

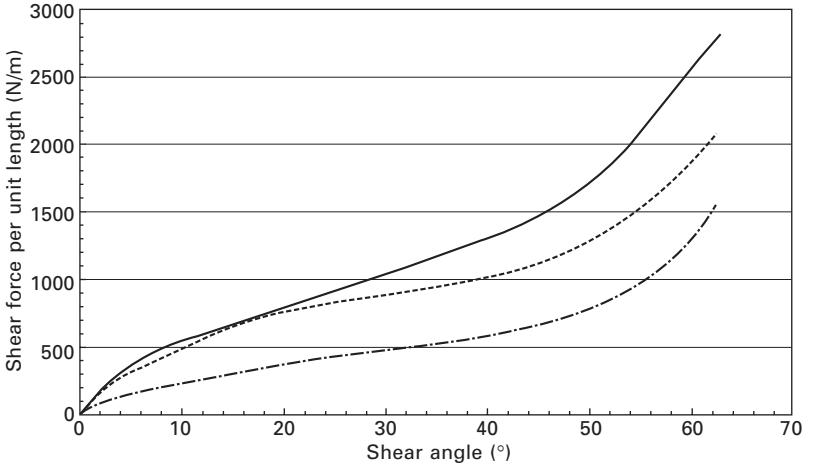

3.8 Picture frame experiments conducted at room temperature at three constant angular shear rates, 0.93, 4.65 and 9.3° s^{-1} (from bottom to top) on a 5-harness satin weave carbon–epoxy prepreg.

are considered inextensible and no inter-tow or crossover slip occurs within the sample, then one can show that the shear angle in region A is always twice that in region B, while region C remains undeformed. The deformation in region A can be considered equivalent to the deformation produced by the pure shear of a picture frame test. The length of the material sample must be at least twice its width in order for the three different deformation regions to exist. Increasing the length/width ratio, λ, to higher values serves to increase the area of region A.

Like picture frame tests, bias extension tests are simple to perform and provide reasonably repeatable results. The test provides an excellent method of estimating a material's locking angle, i.e. the angle at which intra-ply slip (see section 3.2) and/or out-of-plane bending (wrinkling) become significant deformation mechanisms during bias extension tests. A convenient method of detecting the onset of these alternative deformation mechanisms is to monitor the test kinematics. For example, when $\lambda = 2$ the shear angle in region A of Fig. 3.9 should obey eqn (3.20) as long as deformation mechanisms, such as intra-ply slip, are insignificant compared with trellis shearing (Harrison *et al*. 2002c 2004b).

Unlike the picture frame test, as long as the material sample is tightly clamped, the boundary conditions are much less relevant to the test result. Optimum clamping conditions can be achieved by cutting the clamping areas (shown in Fig. 3.9) along the fibre reinforcement directions. Also, owing to the nature of the sample deformation induced by the bias extension test, the influence of relatively cool material adjacent to the metal clamps during high-temperature testing is of less importance than in picture frame tests.

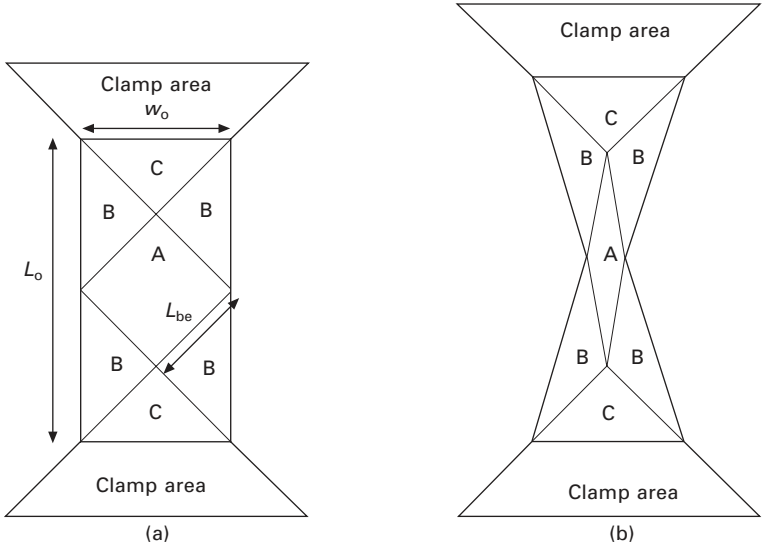

3.9 An idealised bias extension test sample with $\lambda = L_o/w_o = 2$ where L_o and w_o are the initial length and width of the bias extension sample respectively. Region A undergoes pure shear. It can be shown that the shear angle in region B is half that in region A. Region C remains undeformed throughout the test and consequently does not contribute to the shear force. For bias extension tests with $\lambda = 2$, L_{be} is the side length of region A and is used to normalise force, displacement and displacement rates.

However, the test does suffer from certain drawbacks. Firstly, the shear angle and angular shear rate in the material must be measured either by time-consuming visual analysis (which can be complicated further if the sample is to be heated in an oven) or by stopping the test at various displacements and taking measurements from the cooled samples. Secondly, the deformation field within the material is not homogeneous, preventing simple rheological analysis of the results. Finally, the test induces a combination of both pure shear and intra-ply slip. In terms of rheological analysis this presents extra difficulty, though conversely, this deformation may be used to advantage as a means to investigate intra-ply slip as a potential deformation mechanism of woven CFRC. Normalised test results from bias extension tests are presented in section 3.4.3.

3.4.3 Normalisation of characterisation test results

Ideally, the determination of material properties in a characterisation test should be independent of the test method and sample geometry. For example, the shear modulus or shear viscosity (depending on modelling approach) and consequently the shear force produced during the testing of a material should

be independent of both sample dimensions (picture frame and bias extension tests) and length/width ratio (bias extension test). The differences in sample geometry and test kinematics induced by the picture frame and bias extension tests mean that an appropriate normalisation technique must be used before results from different tests can be compared directly.

Normalisation of shear force data from picture frame tests has been considered recently (Harrison *et al*. 2002c, 2004b; Peng *et al*. 2004). Energy arguments have been used to show that, when the shape of the original test specimen is square, i.e. only a small amount of material is missing from the corners of the sample when loaded in the picture frame, force measurements recorded by the picture frame test should be normalised with respect to a characteristic length. A convenient length to use is the side length of the picture frame, L_{pf}. Thus:

$$\frac{F_1}{L_{pf1}} = \frac{F_2}{L_{pf2}} \tag{3.21}$$

where the subscripts 1 and 2 refer to two different picture frames of arbitrary size. Energy arguments can also be applied in normalising bias extension test results. Indeed, bias extension results could be normalised by a characteristic length for comparison between results from tests on different sized samples with the same length/width ratio, λ, conducted at the same shear rate. However, a method of normalising bias extension data for comparison with picture frame tests is less obvious because of the different deformations occurring in the samples of the two experiments. In Harrison *et al*. (2003) an energy argument is presented that involved determining the relative contribution to the deformation energy from regions A and B of a sample of arbitrary length/width ratio (see Fig. 3.10).

The argument is based on a number of simple approximations and so a certain amount of disagreement between normalised data from the picture frame and bias extension experiments is expected. Nevertheless, the bias extension normalisation procedure provides a convenient method of using the two different test methods to check the validity of experimentally produced results. By assuming that the textile composite deforms as a 'constrained Newtonian fluid', the energy argument leads to the following relationship (Harrison *et al*. 2003):

$$\frac{F_{pf}}{L_{pf}} = \frac{(\lambda - 1)}{R(2\lambda - 3 + 2X)} \frac{F_{be}}{L_{be}} \tag{3.22}$$

where F_{be} is the axial force measured by the bias extension test, L_{be} is the characteristic length shown in Fig. 3.10, and

$$X = \frac{1}{4}\left\{\frac{\cos^2\theta[1 + 3\sin^2(\theta/2)}{\cos^2(\theta/2)[1 + 3\sin^2(\theta)}\right\} \tag{3.23}$$

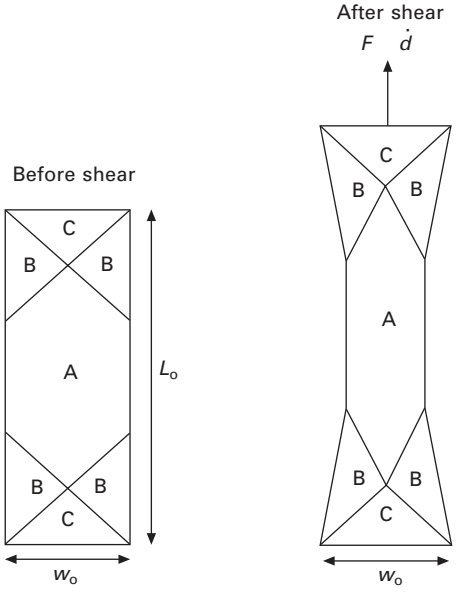

3.10 Bias extension test sample of arbitrary length/width ratio, λ.

and

$$R = \frac{\dot{d}_{be} L_{pf}}{(\lambda - 1)\dot{d}_{pf} L_{be}} \qquad 3.24$$

Error introduced by any non-Newtonian response will become more significant as the ratio R diverges from unity. The above analysis holds only as long as the bias extension test sample follows idealised kinematics. This is a reasonable approximation for low shear angles but begins to fail at higher shear angles because of the occurrence of inter-ply slip in bias extension tests.

In order to plot and compare results of picture frame and bias extension tests it is convenient to define a normalised crosshead displacement that gives an alternative measure of deformation in the material than the shear angle. For the picture frame test this can be defined simply as d_{pf}/L_{pf} whereas for a bias extension test the normalised displacement is defined as $d_{be}/L_{be}(\lambda - 1)$, where d_{be} is the displacement of the crosshead mounting in the bias extension tests. The value of this normalisation technique is illustrated in Fig. 3.11.

Figure 3.11(a) and (b) show comparisons of the normalised force measured using picture frame and bias extension tests on a 2 × 2 twill weave pre-consolidated glass/polypropylene thermoplastic composite (fibre volume fraction = 0.35, melt temperature approximately 160 °C, thickness = 0.54 mm) at 165 and 180 °C and at a normalised displacement rate of 5.7 min^{-1}.

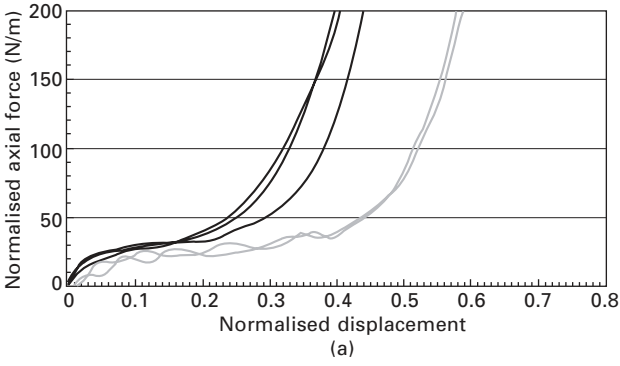

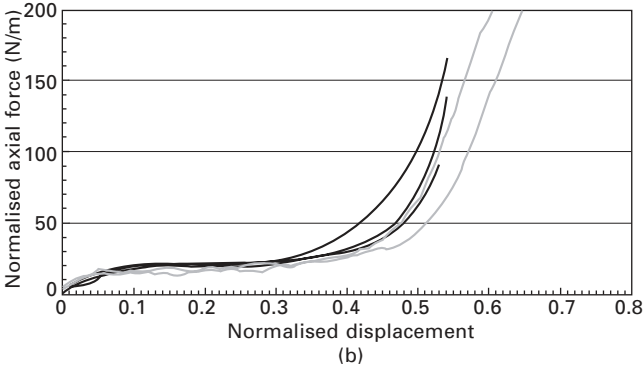

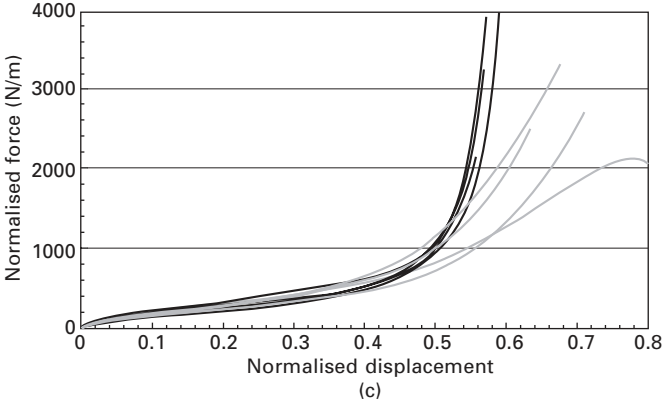

3.11 Normalised picture frame (black lines) and bias extension (grey lines) results for a pre-consolidated glass/polypropylene 2 × 2 twill weave thermoplastic composite at (a) 165 °C and (b) 180 °C and (c) for a 5-harness satin weave carbon/epoxy prepreg at room temperature.

Likewise, Fig. 3.11(c) shows a comparison of the normalised force measured using picture frame and bias extension tests on a thermosetting 5-harness satin weave carbon/epoxy prepreg (fibre volume fraction = 0.55, thickness = 0.5 mm) at room temperature and at a normalised displacement rate of 0.69 min^{-1}. The force data from each experiment were normalised according to the procedures described above. Results are taken from Harrison *et al*. (2004b).

For the thermoplastic composite the normalised force data show excellent agreement at 180 °C but at 165 °C the results diverge at high normalised-displacements. This was because of the cooling effect of the picture frame, an effect that inhibited melting of the material near the metal clamps. Thus the normalisation technique can be used to compare the results of the two tests to check for possible error due to the experimental method. In Fig. 3.11(c) results from experiments on the thermosetting prepreg composite serve to illustrate the large difference in shear force typically produced by a thermosetting prepreg composite (sheared at room temperature) and a thermoplastic composite sheared above its melt temperature (Fig. 3.11a and b).

3.5 Forming evaluation methods

Once appropriate constitutive model parameters (section 3.3) have been determined or evaluated using characterisation tests (section 3.4), they can be implemented in numerical codes (see Chapter 4). Checking the accuracy of the predictions of these forming simulations against formed components provides the final step in validating the whole virtual forming operation. Grid strain analysis and its application in composite sheet forming have been discussed previously (Martin *et al*. 1997a). Here an optical system is reported, known as CAMSYS Automated Strain Analysis and Measurement Environment (ASAME), that can measure strains and fibre shear angles from formed components both efficiently and accurately. This commercial metal forming analysis system has been adapted to determine the deformation of dry fabrics and composites (Long *et al*. 1997, 2002). The procedure is as follows:

1. A square grid with a (known) regular spacing is marked on a sheet of the material to be formed. For 0/90° woven composites, the grid should coincide with the tow directions.
2. A component is formed using the prepared material. Any process can be analysed in theory, as long as the manufacturing route does not obscure the gridlines.
3. Photographs are taken of the formed component. At least two photographs have to be taken of each region of interest. The photographs must also include a target cube, supplied by the manufacturer of the system. The cube allows the processing software to compute the 3D coordinates of each gridline.

4. The photographs are combined and analysed by computer software to compute the coordinates of gridlines and nodes.
5. By computing the angle formed at the intersection of gridlines, intra-ply shear can be calculated.
6. By comparing the gridline spacing with the marked grid, fibre slip or fibre extension can be calculated.

As an example, the system is used to analyse two hemispherical components formed using two different materials by the vacuum forming process. The first material was a double layer of woven thermoplastic commingled glass/polypropylene composite material – a balanced 2 × 2 twill woven fabric of density 1.5 g/cm^3 consisting of a yarn of 60% by mass commingled E-glass and polypropylene, denoted Material A. The second material was a single layer of woven (5-harness satin weave) preimpregnated thermosetting carbon/epoxy material, of density 1.301 g/cm^3, consisting of a tow of 55% by volume carbon fibre with epoxy matrix, denoted Material B. A female mould was used for each component, with a radius of 60 mm.

3.5.1 Shear deformation

Using the optical system, the shear angle distribution for each hemisphere was measured. The results are displayed in Fig. 3.12 for Materials A and B. The distributions are reasonably symmetric between quadrants. Maximum shear occurs along the bias axis of each quadrant. However, Material B (prepreg) exhibits slightly higher levels of shear than Material A (thermoplastic) in the highly deformed regions. The maximum shear angle for the prepreg was 55°, compared with 46° for the thermoplastic. This difference is presumably due to the different rheological behaviours of the two composite materials as well as uncertainties associated with the hand lay-up procedure.

The information captured using this technique can be presented in numerous ways for comparison with numerical simulation results. For example, Fig. 3.13 shows the fibre pattern predicted by a kinematic drape model (KDM). This model does not take any material properties into account and is based on a mapping procedure that calculates the draping of a pin jointed net across the surface of the component. The method incorporates the fibre inextensibility constraint.

In order to visualise graphically the difference in shear angle between the formed components and the kinematic drape predictions, shear angle is plotted along a section of maximum shear in Fig. 3.14. For the hemisphere formed using Material A, two quadrants were analysed. Variation in the two sets of data illustrates the degree of asymmetry in the formed component. For each component, shear angle increases along the section in a manner similar to that predicted by the KDM, until a maximum shear angle is reached at the flange region.

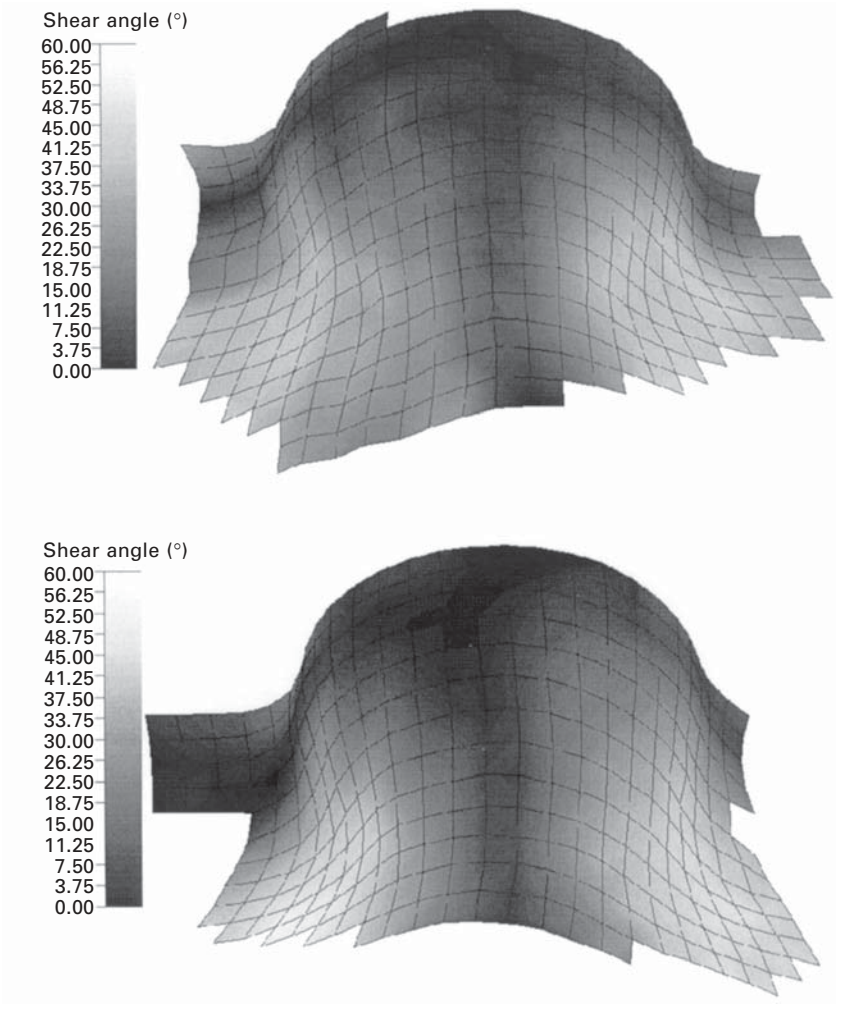

3.12 Shear angle distribution for hemisphere formed from Material A (commingled glass/polypropylene, top) and Material B (carbon/epoxy prepreg, bottom).

As another example, a global picture of the difference in shear angle across the components may be obtained by displaying the frequency with which any particular shear angle occurs. A graph showing such data is presented in Fig. 3.15, along with data for the KDM. Lower shear angles were obtained more frequently for Material B than for Material A, although the range of angles was higher for Material B. The distribution predicted by a kinematic drape simulation covers a wider range of angles than achieved with either material. Lower shear angles (<5°) were predicted more frequently than

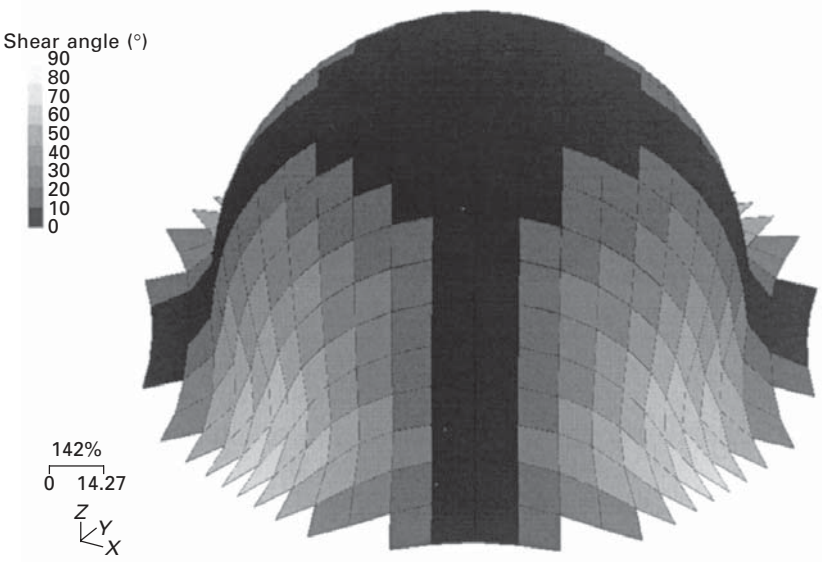

3.13 Shear angle distribution predicted by kinematic drape model. The kinematic drape model is based on a geometric mapping of a pin-jointed fibre network, and ignores material forming rheology when calculating the fibre pattern.

occurred in the experimental measurements, probably due to the difficulty in laying up the material symmetrically (i.e. in practice each quadrant was pre-sheared by a small amount). The predicted distribution is most similar to that obtained using Material B (prepreg). This frequency distribution method of visualising the data can also be used to compare the shear distributions required to form different components, making it a useful design tool in deciding which lay-up or geometry to choose.

3.5.2 Secondary deformation mechanisms

When a textile composite is formed to a 3D shape such as a hemisphere, a number of deformation mechanisms occur (see section 3.2). The primary mechanism is intra-ply shear. However, un-crimping of tows and crossover slip can also contribute to the material deformation. The optical system described here is capable of measuring not just the shear angle between reinforcement directions at any point but also the distance between nodes of the deformed grid (see section 3.5.1). Using this information extension and contraction along the lengths of the reinforcement directions can also be measured. Figure 3.16 shows the extension ratio (final grid spacing divided by initial spacing) experienced by the two materials during forming.

The extension ratio is positive in the region close to the pole of the

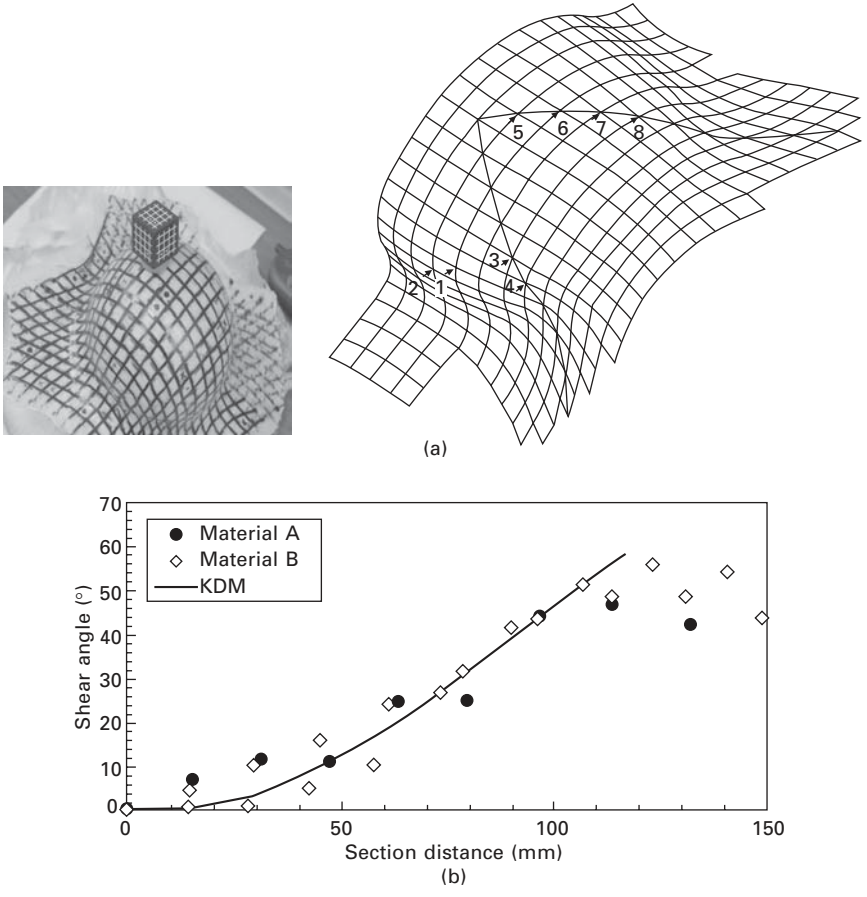

3.14 Validation of predicted fibre patterns for a hemisphere. (a) Lines along sections of maximum shear, with insert showing formed component and measuring cube. (b) Comparison between measured and predicted shear angles along a section of the hemispheres.

hemisphere and negative on the part close to the flange. Positive extension ratio is due to the lay-up of the material over the tool. The material is pushed down into the tool leading to the un-crimping of tows in the region close to the pole. However, yarns close to the flange are pushed together, producing a negative extension ratio. Extension ratios for Material A were in the range 0.78 to 1.24, while those for Material B were 0.87 to 1.10. Although Material A has a large tow width and inter-tow spacing, Material B has a small tow width and little inter-tow spacing. The Material A textile structure facilitates relative movement between tows, leading to higher extension ratios. Similar trends are observed in each direction for the each material. Higher changes in grid spacing were observed for Material A, which would explain the lower shear angles observed for this material. As before, information captured

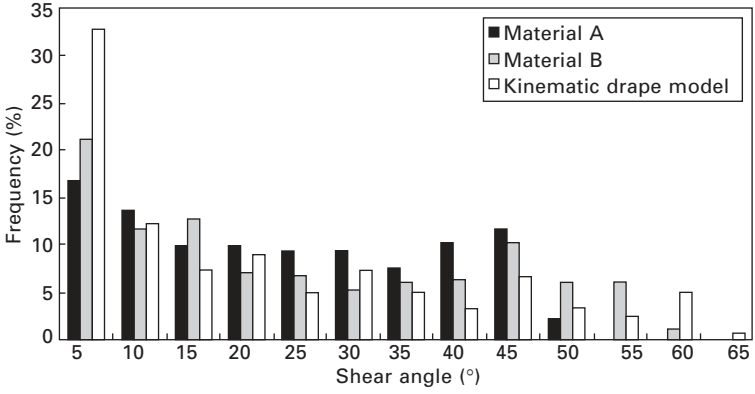

3.15 Frequency distribution comparing shear angles obtained for Material A (commingled fabric) and Material B (prepreg) hemispheres with kinematic drape model predictions.

using this optical technique can be presented in numerous ways for comparison with numerical simulation results. Indeed, observations of material extensions have prompted various workers to perform numerical simulations incorporating extensible fibre reinforcement behaviour (Lamers *et al*. 2002a, 2003; Sharma and Sutcliffe 2003).

3.6 Summary

The rheological modelling and characterisation of viscous textile composites have progressed significantly since 1995. Through incorporation of non-linear material behaviour in continuum models (section 3.3.3), various workers have shown how these materials can be characterised using specialised experimental techniques (section 3.4). However, the number of parameters appearing in these models has meant an extensive number of tests must be performed for each characterisation, which is a long and costly process. A response to this problem has been the use of homogenisation and energy summation techniques, facilitated by recent dramatic increases in computational speed. These methods predict the rheological behaviour of viscous textile composites using knowledge of the composites structure and behaviour of the constituent materials. Methods of evaluating predictions of computer simulations of complex material deformations that implement these rheological models are becoming more sophisticated and rigorous (section 3.5).

3.7 Acknowledgements

We thank the following organisations for their support: EPSRC, BAE SYSTEMS, BP Amoco, ESI Software, Ford Motor Company, QinetiQ, Saint-

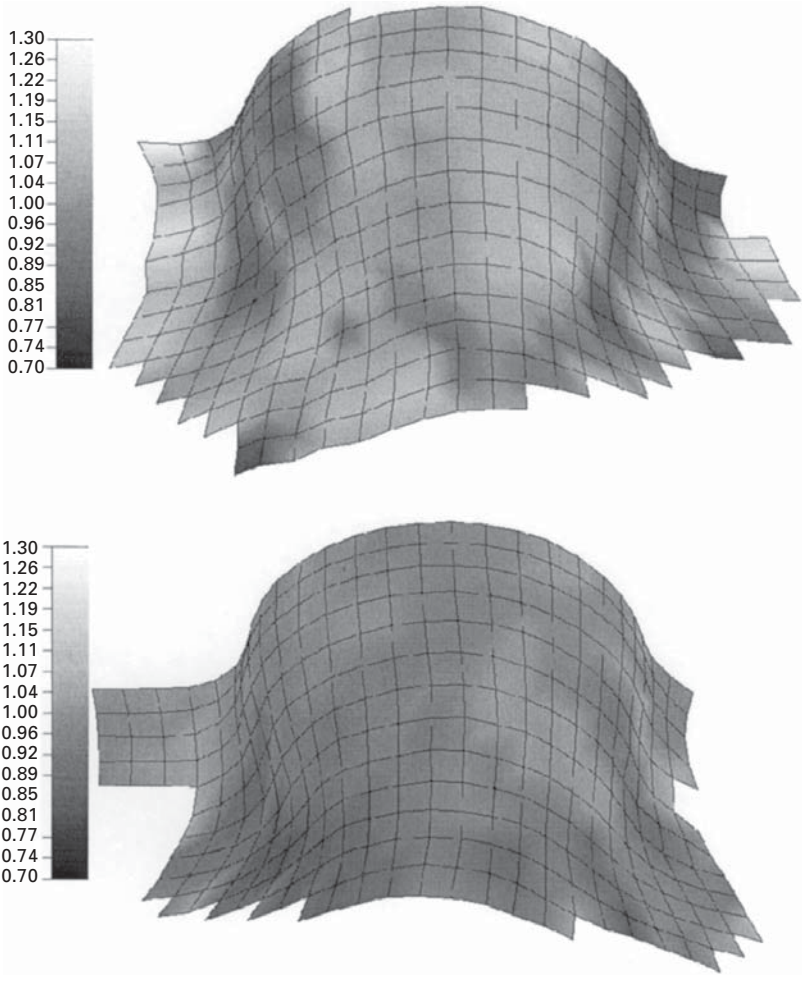

3.16 Extension ratio distribution for a hemisphere formed and consolidated using Material A (thermoplastic, top) and Material B (prepreg, bottom).

Gobain Vetrotex, MSC Software Ltd, and the Universities of Cambridge and Leeds. The authors also thank both Prof. A.J. Spencer and Dr W.R. Yu for helpful discussions on this work. We also acknowledge R. Garcia Gil and M. Sherburn for their contributions.

3.8 References

Advani S.G., Creasy T.S. and Shuler S.F. (1997), *Composite Sheet Forming: Rheology of Long Fiber-reinforced Composites in Sheet Forming*, 323–369, 8, ed. Bhattacharyya D., S.G. Pipes Elsevier, Amsterdam.

Balasubramanyam R., Jones R.S. and Wheeler A.B. (1989), Modelling transverse flows of reinforced thermoplastic materials. *Composites*, 20, 1, 33–37.

Barnes J.A. and Cogswell F.N. (1989), Transverse flow processes in continuous fibre-reinforced thermoplastic composites. *Composites*, 20, 1, 38–42.

Binding D.M. (1991), Capillary and contraction flow of long-(glass) fibre filled polypropylene *Composites Manufacturing*, 2, 3/4, 243–252.

Blanchard P., Cao J., Chen J. and Long A.C. (2001), National Science Foundation Workshop on Composite Sheet Forming, http://www.mech.northwestern.edu/fac/cao/nsfworkshop/index.htm, Lowell, MA, 5–7 September.

Boisse P., Gasser A. and Hivet G. (2001), Analyses of fabric tensile behaviour: determination of the biaxial tension-strain surfaces and their use in forming simulations. *Composites: Part A*, 32, 1395–1414.

Canavan R.A., McGuiness G.B. and O'Bradaigh C.M. (1995), Experimental intraply shear testing of glass-fabric reinforced thermoplastic melts, *4th International Conference on Automated Composites (ICAC '95)*, Nottingham, September, 127–139.

Christensen R.M. (1993), Effective viscous flow properties for fibre suspensions under concentrated conditions. *Journal of Rheology*, 37, 1, 103–121.

Coffin D.W., Pipes R.B. and Simacek P. (1995), First-order approximations for the effective shearing viscosities of continuous-fiber suspensions. *Journal of Composite Materials*, 29, 9, 1196–1180.

Cogswell F.N. (1992), *Thermoplastic Aromatic Polymer Composites*, Butterworth-Heinemann Ltd, Oxford.

Cogswell F.N. (1994), Continuous fibre systems, in *Flow and Rheology in Composite Manufacturing*, 127–144, Ch. 10, Ed. Advani S.G., Pipes R.B., Elsevier, Amsterdam.

Cogswell F.N. and Groves D.J. (1988), The melt rheology of continuous fibre reinforced structural composite materials. *Xth International Congress on Rheology,* Sydney, 275–277.

De Luca P., Lefebure P., Pickett A.K., Voldermayer A.M. and Werner W. (1996), The numerical simulation of press forming of continuous fiber reinforced thermoplastics. *28th International SAMPE Technical Conference*, 4–7, November Seattle, Washington.

De Luca P., Lefebure P. and Pickett A.K. (1998), Numerical and experimental investigation of some press forming parameters of two fibre reinforced thermoplastics: APC2-AS4 and PEI-CETEX. *Composites Part A*, 29A, 101–110.

Dykes R.J., Martin T.A. and Bhattacharyya, D. (1998), Determination of longitudinal and transverse shear behaviour of continuous fibre-reinforced composites from vee-bending. *Composites Part A*, 29A, 39–49.

Friedrich K., Hou M. and Krebs J. (1997), *Composite Sheet Forming: Thermoforming of Continuous Fibre/Thermoplastic Composite Sheets*, 91–162, Ch. 4, Ed. Bhattacharyya D., Pipes S.G., Elsevier, Amsterdam.

Goshawk J.A. and Jones R.S. (1996), Structure reorganisation during the rheological charaterisation of continuous fibre-reinforced composites in plane shear. *Composites Part A*, 27A, 279–286.

Goshawk J.A., Navez V.P. and Jones R.S. (1997), Squeezing flow of continuous fibre-reinforced composites. *Journal of Non-Newtonian Fluid Mechanics*, 73, 327–342.

Groves D.J. (1989), A characterisation of shear flow in continuous fibre thermoplastic laminates. *Composites*, 20, 1, 28–32.

Groves D.J. and Stocks D.M. (1991), Rheology of thermoplastic composite carbon fibre composite in the elastic and viscoelastic states. *Composites Manufacturing*, 2, 3/4, 179–184.

Hagege B., Boisse P. and Billoet J.L. (2003), Specific simulation tools for the shaping process of knitted reinforcements. *6th International ESAFORM Conference on Materials Forming*, 28–30 April, Salerno, 871–874.

Harrison P., Clifford M.J., Long A.C. and Rudd C.D. (2002a), Constitutive modelling of impregnated continuous fibre reinforced composites: a micro-mechanical approach. *Plastics, Rubber and Composites*, 2, 31, 76–86.

Harrison P., Clifford M.J., Long A.C. and Rudd C.D. (2002b), A micro-mechanical constitutive model for continuous fibre reinforced impregnated composites. *5th International ESAFORM Conference on Materials Forming*, 15–17 April, Krakow, 275–278.

Harrison P., Clifford M.J. and Long A.C. (2002c), Shear characterisation of woven textile composites, *10th European Conference on Composite Materials*, 3–7 June, Brugge.

Harrison P., Long AC., Clifford M.J., Garcia Gil R., Ward I.M. and Hine P.J. (2002d), Investigation of thermoformability and molecular structure of Curv™: *Automotive Composites and Plastics*, 3–4 December, Basildon, ESSEX, UK.

Harrison P., Clifford M.J., Long A.C. and Rudd C.D. (2003), Constitutive modelling of shear deformation for impregnated textile composites. *6th International ESAFORM Conference on Materials Forming*, 28–30 April, Salerno, 847–850.

Harrison P., Clifford M.J., Long A.C. and Rudd C.D. (2004a), A constituent based predictive approach to modelling the rheology of viscous textile composites. *Composites: Part A* 38, 7–8, 915–931.

Harrison P., Clifford M.J. and Long A.C. (2004b), Shear characterisation of woven textile composites: a comparison between picture frame and bias extension experiments. *Composites Science and Technology*, 64, 10–11, 1453–1465.

Hsiao S.W. and Kikuchi N. (1999), Numerical analysis and optimal design of composite thermoforming process. *Computing Methods in Applied Mechanical Engineering*, 177, 1–34.

Hull B.D., Rogers T.G. and Spencer A.J.M. (1991), Theory of fibre buckling and wrinkling in shear flows of fibre-reinforced composites. *Composites Manufacturing*, 2, 3/4.

Hull B.D., Rogers T.G. and Spencer A.J.M. (1994), Theoretical analysis of forming flows of continuous fibre resin systems. *Flow and Rheology in Composite Manufacturing*, 203–256, Ch. 10, Ed. Advani S.G., Pipes R.B., Elsevier, Amsterdam.

Johnson, A.F. (1995), Rheological model for the forming of fabric reinforced thermoplastic sheets. *Composites Manufacturing*, 6, 153–160.

Jones R.S. and Roberts R.W. (1991), Ply reorientation in compression. *Composites Manufacturing*, 2, 3/4, 259–266.

Lai C.L. and Young W.B. (1999), Modelling fibre slippage during the preforming process. *Polymer Composites*, 20, 4, 594–603.

Lamers E.A.D., Akkerman R. and Wijskamp S. (2002a), Fibre orientation modelling for rubber press forming of thermoplastic laminates. *5th International ESAFORM Conference on Material Forming*, Krakow, 323–326, 14–17, April.

Lamers E.A.D., Akkerman R. and Wijskamp S. (2002b), Drape modelling of multi-layer fabric reinforced thermoplastic laminates. *Proc. 6th International Conference on Textile Composites (TexComp 6),* Philadelphia, USA, September.

Lamers E.A.D., Wijskamp S. and Akkerman R. (2003), Drape modelling of multi-layered composites. *6th International ESAFORM Conference on Material Forming*, Salerno, 823–826, 28–30, April.

Lebrun G. and Denault J. (2000), Influence of the temperature and loading rate on the intraply shear properties of a polypropylene fabric. *15th American Association for*

composites, 25–27 September, College Station, Texas, 659–667.
Lebrun G., Bureau M.N. and Denault J. (2003), Evaluation of bias-extension and picture-frame test methods for the measurement of intraply shear properties of PP/glass commingled fabrics. *Composite Structures*, 61, 341–352.
Li H. and Gutowski T. (1997), *Composite Sheet Forming: The Forming of Thermoset Composites*, 441–472, Ch. 11, Ed. Bhattacharyya D., Pipes S.G., Elsevier, Amsterdam.
Lomov S.V., Belov E.B. and Verpoest I. (2002), Behaviour of textile reinforcement in composite forming: mathematical modelling of deformability, internal geometry and permeability of the perform. *5th International ESAFORM Conference on Material Forming*, Krakow, Poland, 271–274, 14–17, April.
Long A.C. Rudd C.D., Blagdon M. and Johnson M.S. (1997), Experimental analysis of fabric deformation mechanisms during preform manufacture. *Proc. 11th International Conference on Composite Materials (ICCM-11),* Gold Coast, Australia, 5, July, 238–248.
Long A.C., Gil R.G., Clifford M.J., Harrison P., Sharma S.B. and Sutcliffe M.P.F. (2002), Experimental analysis of fabric deformation during forming of textile composites. *5th International ESAFORM Conference on Material Forming,* Krakow, Poland, 279–282, 14–17, April.
Lussier D. and Chen J. (2000), Material characterisation of woven fabrics for thermoforming of composites. *15th American Association for Composites*, 25–27 September, College Station, Texas, 301–310.
Lussier D.S., Chen J. and Sherwood J.A. (2002), Viscosity based models for shear of glass/thermoplastic fabrics. *5th International ESAFORM Conference on Material Forming*, Krakow, Poland, 283–286, 14–17, April.
Mallon P.J. and O'Bradaigh C.M. (2000), in *Comprehensive Composite Materials, Volume 2: Polymer Matrix Composites*, Eds Talreja R., Manson J.A.E., Series eds Kelly A., Zweben C., Elsevier, Amsterdam, 874–913.
Mander S.J. (1998), Roll forming of fibre reinforced thermoplastic composites. PhD Thesis, University of Auckland, New Zealand.
Mander S.J., Panton S.M., Dykes R.J. and Battacharyya D. (1997), *Composite Sheet Forming: Roll Forming of Sheet Materials*, 473–515, Ch. 12, Ed. Bhattacharyya D., Pipes S.G. Elsevier, Amsterdam.
Martin T.A., Bhattacharyya D. and Collins I.F. (1995), Bending of fibre-reinforced thermoplastic sheets. *Composites Manufacturing*, 6, 177–187.
Martin T.A., Christie G.R. and Bhattacharyya D. (1997a), *Composite Sheet Forming: Grid Strain Analysis and its Application in Composite Sheet Forming*, 217–245, Ch. 6, Ed. Bhattacharyya D., Pipes S.G. Elsevier, Amsterdam.
Martin T.A., Mander S.J., Dykes R.J. and Bhattacharyya D. (1997b), *Composite Sheet Forming: Bending of Continuous Fibre-Reinforced Thermoplastic sheets*, 371–401, Ch. 9, Ed. Bhattacharyya D., Pipes S.G. Elsevier, Amsterdam.
McEntee S.P. and O'Bradaigh C.M. (1998), Large deformation finite element modelling of single-curvature composite sheet forming with tool contact. *Composites Part A*, 29A, 207–213.
McGuiness G.B. and O'Bradaigh C.M. (1997), Development of rheological models for forming flows and picture frame testing of fabric reinforced thermoplastic sheets. *Journal of Non-Newtonian Fluid Mechanics*, 73, 1–28.
McGuiness G.B. and O'Bradaigh C.M. (1998), Characterisation of thermoplastic composite melts in rhombus-shear: the picture frame experiment. *Composites Part A*, 29A, 115–132.

McGuiness G.B., Canavan R.A., Nestor T.A. and O'Bradaigh M.O. (1995), A picture frame intra-ply sheet forming of composite materials. *Proceedings of the American Society of Mechanical Engineers (ASME) Materials Division,* ASME, 1107–1118.

Milani A.S., Nemes J.A., Pham X.T. and Lebrun G. (2003), The effect of fibre misalignment on parameter determination using picture frame test. *Proc. 14th International Conference on Composite Materials (ICCM-14*), San Diego, US, July.

Murtagh A.M. and Mallon P.J. (1995), Shear characterisation of unidirectional and fabric reinforced thermoplastic composites for pressforming applications. *Proc. 10th International Conference on Composite Materials (ICCM-10)*, Whistler, Canada, 373–380, August.

Murtagh A.M. and Mallon P.J. (1997), *Composite Sheet Forming: Characterisation of Shearing and Frictional Behaviour during Sheet Forming*, 163–216, 5, Eds Bhattacharyya D., Pipes S.G., Elsevier, Amsterdam.

O'Bradaigh C.M. and Pipes R.B. (1991), Finite element analysis of composite sheet-forming process. *Composites Manufacturing*, 2, 3/4, 161–170.

O'Bradaigh C.M., McGuiness G.B. and McEntee S.P. (1997), *Composite Sheet Forming: Implicit Finite Element Modelling of Composites Sheet Forming Processes*, 247–322, Ch. 7, Eds Bhattacharyya D., Pipes S.G., Elsevier, Amsterdam.

Peng X.Q. and Cao J. (2002), A dual homogenization and finite element approach for material characterization of textile composites. *Composites: Part B*, 33, 45–56.

Peng X.Q., Cao J., Chen J., Xue P., Lussier D.S. and Liu L. (2004), Experimental and numerical analysis on normalization of picture frame tests for composite materials. *Composites Science and Technology*, 64, 11–21.

Phung T., Paton R. and Mouritz A.P. (2003), Characterisation of interply shearing resistance of carbon–epoxy unidirectional tape and fabric prepregs. *6th International ESAFORM Conference on Materials Forming*, 28–30 April, Salerno, Italy, 867–870.

Pickett A.K., Queckborner T., De Luca P. and Haug E. (1995), An explicit finite element solution for the forming prediction of continuous fibre-reinforced thermoplastic sheets. *Composites Manufacturing*, 6, 237–243.

Pipes R.B. (1992), Anisotropic viscosities of an orientated fibre composite with a power law matrix. *Journal of Composite Materials*, 26, 10.

Potter K. (2002), Bias extension measurements on cross-plied unidirectional prepreg. *Composites Part A*, 33, 63–73.

Prosser W., Hine P.J. and Ward I.M. (2000), Investigation into thermoformability of hot compacted polypropylene sheet. *Plastics, Rubber and Composites*, 29, 8, 401–410.

Roberts R.W. and Jones R.S. (1995), Rheological characterisation of continuous fibre composites in oscillatory flow. *Composites Manufacturing*, 6, 161–167.

Rogers T.G. (1989a), Rheological characterisation of anisotropic materials. *Composites*, 20(1), 21–27.

Rogers T.G. (1989b), Squeezing flow of fibre reinforced viscous fluids. *Journal of Engineering Mathematics*, 23, 81–89.

Rogers T.G. (1990), Shear characterisation and inelastic torsion of fibre reinforced materials', in *Inelastic Deformation of Composite Materials*, ed. Dvorak G.J., Springer-Verlag, New York.

Rogers T.G. and O'Neill J.M. (1991), Theoretical analysis of forming flows of fibre-reinforced composites. *Composites Manufacturing*, 2, 3/4, 153–160.

Scobbo J.J. and Nakajima N. (1989), Dynamic mechanical analysis of molten thermoplastic/continuous graphite fiber composites in simple shear deformation. *21st International*

Society for the Advancement of Materials and Process Engineering (SAMPE-21) Technical Conference, 25–28, September, Atlantic City, New Jersey.

Sharma S.B. and Sutcliffe M.P.F. (2003), A simplified finite element approach to draping of woven fabric. *6th International ESAFORM Conference on Materials Forming*, 28–30 April, Salerno, 887–890.

Shuler S.F. and Advani S.G. (1996), Transverse squeeze flow of concentrated aligned fibers in viscous fluids. *Journal of Non-Newtonian Fluid Mechanics*, 65, 47–74.

Smiley A.J. and Pipes R.B. (1988), Analyses of the diaphragm forming of continuous fiber reinforced thermoplastics. *Journal of Thermoplastic Composite Materials*, 1, 298–321.

Spencer A.J.M. (1971), Theory of invariants, in *Continuum Physics*, Ed. Eringen A.C., Academic Press, New York, 240–353.

Spencer A.J.M. (1972), *Deformation of Fibre-reinforced Materials*, Clarendon Press, Oxford.

Spencer A.J.M. (1984), *Continuum Theory for Strongly Anisotropic Solids,* CISM Courses and Lectures No. 282, Spinger-Verlag, New York.

Spencer A.J.M. (2000), Theory of fabric-reinforced viscous fluids. *Composites Part A*, 31, 1311–1321.

Sutcliffe M.P.F., Sharma S.B., Long A.C., Clifford M.J., Gil R.G., Harrison P. and Rudd C.D. (2002), A comparison of simulation approaches for forming of textile composites. *5th International ESAFORM Conference on Materials Forming*, 15–17 April, Krakow, 311–314.

Wheeler A.B. and Jones R.S. (1991), A characterisation of anisotropic shear flow in continuous fibre composite materials. *Composites Manufacturing*, 3/4, 192–196.

Wheeler A.B. and Jones R.S. (1995), Numerical simulation of fibre reorientation in the consolidation of a continuous fibre composite material. *Composites Manufacturing*, 6, 263–268.

Wilks C.E., Rudd C.D., Long A.C. and Johnson C.F. (1999), Rate dependency during processing of glass/thermoplastic composites. *Proc. 12th International Conference on Composite Materials (ICCM-12)*, Paris.

Xue P., Peng X. and Cao J. (2003), A non-orthogonal constitutive model for characterising woven composities. *Composites Part A*, 34, 183–193.

Yu W.R., Pourboghrat F., Chung K., Zampaloni M. and Kang T.J. (2002), Non-orthogonal constitutive equation for woven fabric reinforced thermoplastic composites. *Composites Part A*, 33, 1095–1105.

Yu W.R., Zampaloni M., Pourboghrat F., Chung K. and Kang T.J. (2003), Sheet hydroforming of woven FRT composites: non-orthogonal constitutive equation considering shear stiffness and undulation of woven structure. *Composite Structures*, 61, 353–362.

Yu X., Zhang L. and Mai Y.W. (2000), Modelling and finite element treatment of intra-ply shearing of woven fabric. *International Manufacturing Conference in China (IMCC 2000)*, 16–17 August, Hong Kong.

Zheng Q.S. (1994), Theory of representations for tensor functions. *Applied Mechanical Review*, 47, 554–587.

Zouari B., Dumont F., Daniel J.L. and Boisse P. (2003), Analyses of woven fabric shearing by optical method and implementation in a finite element program. *6th International ESAFORM Conference on Materials Forming*, 28–30 April, Salerno, Italy, 875–878.

4

Forming textile composites

W-R YU, Seoul National University, Korea and
A C LONG, University of Nottingham, UK

4.1 Introduction

This chapter describes modelling approaches for forming of textile composite sheets into three-dimensional components. Forming processes considered here involve both dry fabrics (for liquid moulding) and pre-impregnated composites. A number of simulation techniques exist within the research community, and several of these have been implemented within commercial software packages. The aim of these models is to predict the fibre orientations within the formed component, from which additional information can be deduced, e.g. ply templates for net-shape forming, component thicknesses (for prepreg) or fibre volume fractions (for dry fabric), and composite mechanical properties. Virtually all the work in this field has concentrated on fabrics with two orthogonal fibre directions (i.e. bidirectional fabrics and their composites), and hence this description applies exclusively to such materials. Two modelling approaches are described in detail in this chapter. The first is based on a simple mapping procedure, and the second on a mechanical approach utilising finite element (FE) analysis.

4.2 Mapping approaches

4.2.1 Kinematic models

A number of researchers have developed kinematic simulations of draping or forming for textile reinforcements[1–4]. Several of these models have been implemented within commercially available software packages (e.g. MSC.Patran Laminate Modeler[5], Vistagy FiberSIM[6]). In this approach, the fabric is modelled as a pin-jointed net (or 'fishnet'), which is mapped onto the surface of the forming tool by assuming that tow segments are able to shear at the joints (tow crossovers). A unique draped pattern can be obtained by specifying two intersecting tow paths, referred to as generators, on the surface of the forming tool. The remaining tows are positioned using a

mapping approach, which involves solving geometric equations to determine the intersection of the surface with possible crossover points for the tow segments. Several strategies are available for specifying the generator paths, with either geodesic or projected paths used typically. Correct specification of the generators is critical, as these will determine the positions of all remaining tows. An example of this type of analysis is shown in Fig. 4.1,

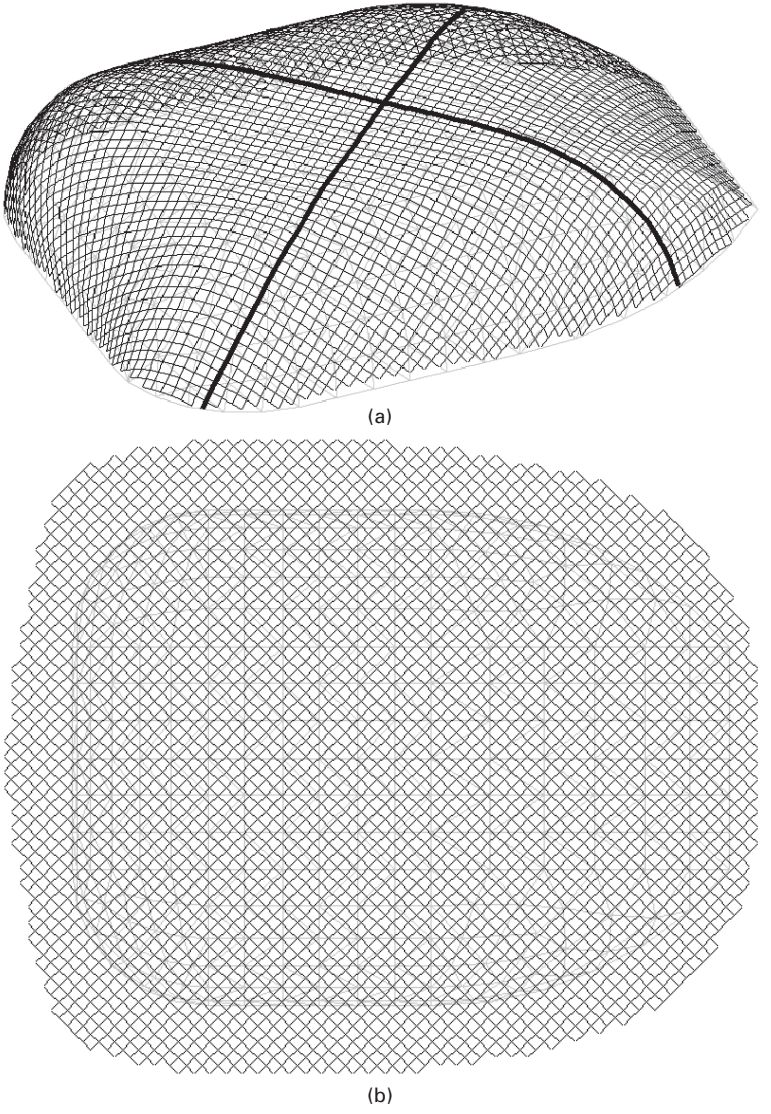

4.1 An example of kinematic draping simulation. (a) Draped fibre pattern based on geodesic generator paths (marked in bold). (b) Predicted net-shape for ± 45° ply.

which illustrates the predicted fibre pattern obtained using a kinematic model with geodesic generator paths. Also shown is the predicted net-shape, which can be used as a ply cutting template.

The kinematic approach provides a very fast solution, with typical run times of less than 10 seconds for complex components. Commercial packages have established interfaces with computer-aided design (CAD) and mesh generation software, and interfaces with ply cutting and placement (laser guide) systems also exist. However, as stated above the solution is dependent on accurate specification of the generator paths. In practice these may be affected by material and process boundary conditions. One other issue is that purely kinematic models are unable to differentiate between materials other than in the specification of the locking angle, which is used to indicate possible areas of wrinkling. Consequently an identical fibre pattern is obtained, regardless of variations in material forming characteristics or processing technique. Nevertheless the ease of use of commercially available kinematic models has meant that they are used widely by composites manufacturers, notably in the aerospace and high-performance automotive (e.g. Formula 1) sectors.

4.2.2 Iterative draping simulation

Generally the geometric/kinematic approach to drape simulation works well for symmetric shapes draped with balanced materials. However for non-symmetric geometries, correct placement of the two generator tow paths may be problematic, and it may not be possible to identify their positions intuitively. In addition, as has been shown in Chapter 2, materials such as non-crimp fabrics (NCFs) exhibit a preferential direction for deformation. This means they are more difficult to shear in one direction, with shear forces for a given shear angle typically up to five times higher for shearing parallel to the stitch than for shearing perpendicular to the stitch. A typical example of this is shown in Fig. 4.2, which shows the shear resistance for a ±45° glass fabric retained using a tricot stitch.

During preform manufacture with NCFs, the resulting fibre pattern may be different from that obtained using a balanced fabric. The use of a mechanical forming simulation would allow consideration of material directionality, as described in section 4.3.3, although this requires a significant level of expertise and increased computation time. The alternative approach presented here is based on the use of a geometric mapping algorithm within an iterative scheme (an approach first suggested by Bergsma[3]). The energy required to produce each mapping is calculated, with the mapping resulting in the lowest energy assumed to represent the actual behaviour of the fabric. In reality the deformation energy is the sum of several components, although here only intra-ply (in-plane) shear resistance is considered, as this is thought to be

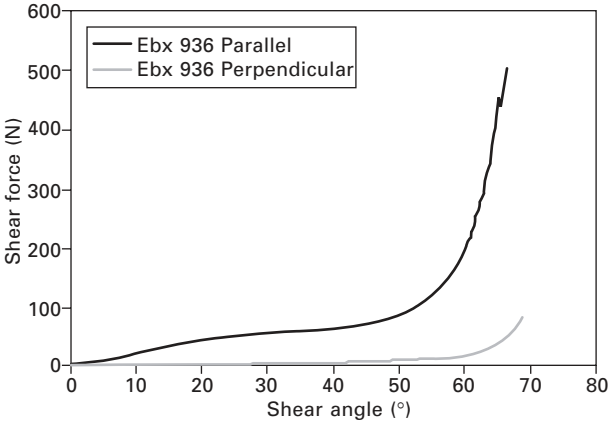

4.2 Shear force versus shear angle curves for a ±45° glass NCF with a tricot stitch, sheared both parallel and perpendicular to the stitching direction.

most indicative of the effect of fabric construction on deformation.

The fabric shear energy (work done during shearing, U_s) can be calculated simply from the area under the torque-shear angle curve:

$$U_s(\theta) = \int_0^{\theta} T(\gamma)\,\mathrm{d}\gamma \qquad 4.1$$

where $T(\gamma)$ is the torque required to achieve a shear angle γ. This expression can be evaluated by fitting an empirical relationship to the shear force versus shear angle curve, measured for example using a picture frame shear test (see Chapter 2). For NCFs, two curves may be specified to represent shearing parallel and perpendicular to the stitching thread. The total energy is calculated within the drape simulation by summing the contribution at each node (tow crossover).

A simple way to determine the mapping resulting with the minimum energy is to use an iterative scheme based on the two generator tow paths. This approach involves finding the two intersecting paths that result in the lowest total energy. A Hooke and Jeeves minimisation method is used[7], where the generator path is defined one step at a time from a user-defined starting point. Each successive set of nodes is positioned by iterating the generator path angle to achieve the minimum increase in shear energy. For reasons of computational efficiency, this technique is preferred to a global minimisation algorithm in which the entire generator path is modified at each stage of the process. However as nodes in contact with the tool are subject to additional constraints due to friction, the present approach is likely to be reasonably accurate.

The above algorithm has been implemented within the 'DrapeIt' software package at the University of Nottingham (as described in detail by Souter[8]). An automotive component is used here to evaluate and to validate the model. The geometry is based on a transmission tunnel for a high-performance vehicle, produced by resin transfer moulding (RTM). Preforms were produced by hand lay-up over a male former. An arrangement of several discrete forming pads was developed to hold the fabric onto the component surface during lay-up. These assisted in the lay-up process and resulted in improved repeatability during preform manufacture. Figure 4.3 compares predicted fibre patterns for this geometry obtained using a variety of techniques. Figure 4.3(a) was obtained using a purely kinematic algorithm with geodesic generator paths. Figure 4.3(b) was generated using the energy minimisation algorithm with shear data for a plain weave fabric. It is clear that the energy minimisation algorithm has reduced the shear deformation over the surface significantly compared with the kinematic model; if the shear strain energies for each simulation are analysed, a reduction of 35% is recorded. Figure 4.3(c) was generated using shear data for a ±45° carbon NCF, having similar shear compliance data to that given in Fig. 4.2. In this case fabric deformation was increased in quadrants that were sheared in the preferential direction.

Figure 4.4 compares predicted and measured shear angles along the length of the component for the NCF. Fabric layers were marked with an orthogonal grid, and shear angles were determined by measuring the relative position of grid points using digital vernier callipers. The results agree over the majority of the length, although the model over-estimates the shear deformation at the rear of the tunnel. For experimentally produced preforms, wrinkles were present in this location. Darts (triangular cuts) were used to alleviate wrinkling, reducing the overall shear deformation in the region. These discontinuities were not represented in the forming simulation.

From the above it may be concluded that software packages based on a kinematic mapping approach are easy to use, and that they can provide a fast and accurate solution for relatively simple geometries. Where either the component or material behaviour is non-symmetric, an iterative energy-based mapping may provide greater accuracy. Nevertheless this approach is still a simplification when compared with the real process. Specifically, it does not consider all the boundary conditions or material properties that are relevant to real forming processes. For example an automated process may include a pinching frame or blank-holder to support the material and to suppress wrinkling. Thermoplastic composites usually require a non-isothermal forming process, where material properties will change as the material is cooled during forming. Such material behaviour and boundary conditions may require the use of a mechanical modelling approach, as described in the following section.

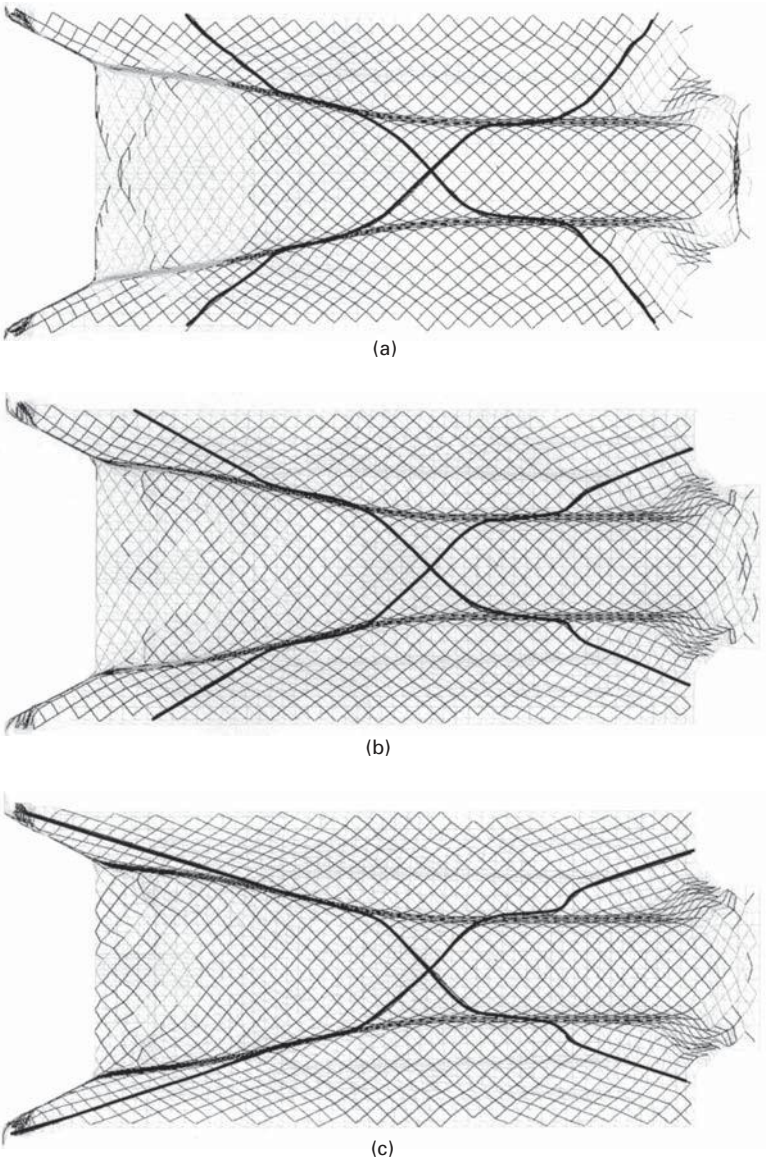

4.3 Predicted fibre patterns for an automotive transmission tunnel. (a) Geometric mapping with geodesic generator paths. (b) Iterative analysis with shear data for a plain weave. (c) Iterative analysis with shear data for a ±45° tricot stitched NCF.

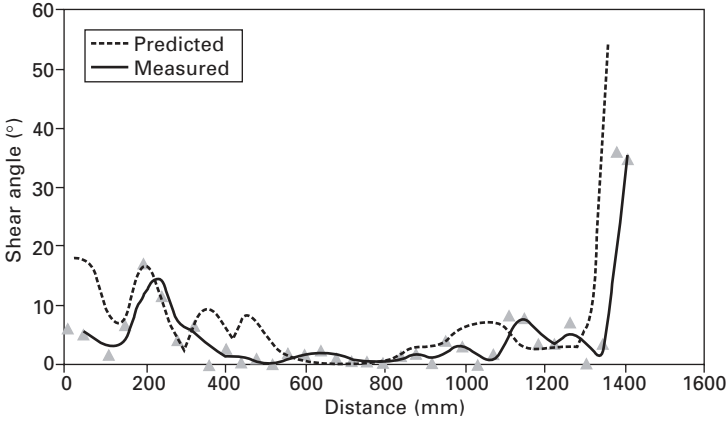

4.4 Comparison of predicted and measured shear angles along the length of the transmission tunnel draped with a ±45° tricot stitched NCF. Measurements were taken along the centre line from left to right with reference to Fig. 4.3(c).

4.3 Constitutive modelling approach

4.3.1 Introduction

In developing composites manufacturing processes, process engineers need to analyse the full forming process, considering factors such as tool configuration and processing conditions. This requires detailed analysis of the material during the forming process, considering material behaviour and process variables. For this purpose the FE method is considered useful, despite long computation times and requirements for an in-depth knowledge of FE analysis and constitutive models. This is because it can predict the final formed shape including stress and strain distributions, and the effects on these from the tool configuration and its interaction with the material. For FE modelling and analysis, constitutive equations are required to describe the mechanical behaviour of the material during forming. This is dependent on the reinforcement structure and (for prepreg) the matrix rheology. Mechanical behaviour of dry fabrics and prepreg were described in detail in Chapters 2 and 3 respectively. In this chapter, constitutive modelling for continuous fibre reinforced composites will be discussed, along with its application to forming simulation.

Fabric-based composites not only improve mechanical and physical properties but also enable rapid, automated production of composite structures. Numerous manufacturing processes have been proposed over the years to shape composite prepreg or preforms, ranging from compression moulding to diaphragm forming and hydroforming. Owing to their high success with metals, various attempts have also been made to apply sheet forming techniques

to composites[9, 10]. One difficulty here is the limited draping capability of fabrics, which are prone to wrinkling. To design an appropriate sheet forming process for fabric-based composites, significant research on constitutive modelling for woven structures has been performed. This can be classified into two general categories: continuum mechanics and non-continuum mechanics-based models. The non-continuum approach can be used for modelling of textile preforms without resin. This enables draping simulations before resin injection during RTM, with (for example) particle dynamics representing the intersection point between warp and weft threads[11].

For continuous fibre reinforced composite forming analysis, the continuum-based approach is preferred because of its ability to model complex deformation behaviour. In general, for composite modelling the material can be treated as either homogeneous or non-homogeneous. Based on non-homogeneous concepts, truss and shell (membrane) elements can be used to model the textile structure and resin matrix, respectively[12, 13]. In this meso-cell approach, the microstructural interaction between the matrix and the reinforcement is accounted for by using common nodes to define the truss and shell (or membrane) elements. Therefore, the meso-cell approach can account for the evolution of the microstructure during forming. However, since this approach takes a large amount of computation and pre-processing time, the homogeneous continuum approach is usually preferred.

Many models assuming homogeneous material properties have been developed, utilising well-defined mathematical theories (such as orthotropic constitutive equations), thereby reducing the computational cost (e.g. Dong *et al.*[14]). These studies assume the preservation of the initial orthotropy of the fabric during forming, which is common practice in sheet metal forming analysis. This assumption is not accurate for the analysis of fabric-based composites, since the change in fibre angle is significant and hence the principal material directions change as the material is formed. Several efforts have been made to develop numerical models capable of capturing this fibre angle evolution. This has resulted in non-orthogonal continuum-based constitutive equations for unidirectional composites that with fibre inextensibility and incompressibility assumptions[15] based on the *ideal fibre reinforced model* (IFRM)[16, 17]. This approach has been applied to diaphragm forming analysis for unidirectional thermoplastic composites[18], and has recently been extended to thermoplastic composites with woven fabric reinforcements[19].

A great deal of research has been devoted to the use of homogenisation methods to account for the evolution of microstructural parameters and also to predict the macroscopic deformed shape of composites. Homogenisation methods involve modelling a unit cell in 3D and then solving a set of governing equations to obtain the homogenised material properties of the composite based on a geometric description of the unit cell[20]. In spite of the computational

disadvantages, including long computational times, the homogenisation method has been used to model a multitude of domains such as the micro-level of the fibre and the meso-level of the fabric[21]. Recently, a new method has been developed that reduces computational cost and accounts for microstructural effects on the forming behaviour of thermoplastic composites. The method utilises numerical techniques to extract non-linear elastic material properties based on the homogenisation method under a continuum mechanics framework[22]. An extensive review of constitutive modelling and its application to forming analysis is provided by Lim and Ramakrishna[23].

In order to simulate forming behaviour, constitutive models are usually implemented within FE software. Since commercial FE software such as ABAQUS[24], MARC[25], PAM-FORM[26] and LS-DYNA[27] are able to model non-linear behaviour, including material and geometric (contact) non-linearity, it is beneficial to use such software. Here, two solution schemes are available: the implicit and explicit FE methods. Although analyses for some simple forming problems can utilise the implicit method, the increase in complexity of forming problems brings with it a number of difficulties, particularly variable contact conditions. For this reason the explicit approach is preferable for forming simulation of textile composites[28, 29]. Implicit and explicit FE methods are described in detail in Chapter 8 in the context of composite mechanical behaviour.

4.3.2 Non-orthogonal constitutive model

It is the shearing mechanism that enables bidirectional fabrics to conform onto the tool during sheet forming, because fibres in tows are very stiff and can be assumed to be inextensible (apart from a small initial extension in woven fabrics due to fibre straightening or 'uncrimping'). Because of shearing, material axes represented by the warp and weft directions become non-orthogonal. Before discussing a method to treat the non-orthogonal nature of the material axes, the limitations of an orthotropic assumption of material axes are discussed to emphasise the necessity for a non-orthogonal constitutive equation.

As an example, a square sheet of woven composite was subjected to a shear boundary force on its right-hand edge while the left-hand edge was constrained not to move in the x-direction but was free to move in the y-direction. To prevent rigid body motion of the sheet, the lower left corner was completely fixed as shown in Fig. 4.5(a). A total of 10×10 rectangular plane stress elements were used with an orthotropic, elastic constitutive equation. A small shear modulus was used with large Young's moduli in both the x and y material directions. The predicted shape in Fig. 4.5(b) shows a significant change in length of the left edge. This length change comes from the assumption that the material axes remain orthogonal during deformation

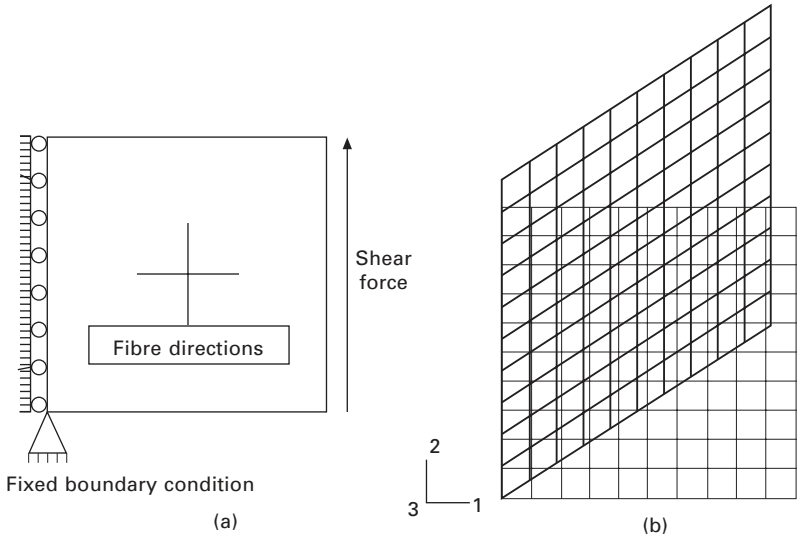

4.5 Simple shear simulation[30]. (a) Geometry and boundary condtions. (b) Deformed shape using orthotropic constitutive equation (E_{11} = 19 GPa, E_{22} = 19 GPa, v = 0.1, G = 0.01 MPa).

(they can rotate, but remain orthogonal). This issue is discussed in more detail by Yu *et al.*[30]

Given the obvious problems associated with the orthotropic material law, several approaches have been proposed to predict deformation behaviour of bidirectional textiles. Structural elements are often used to represent the tows within the fabric structure, for example one-dimensional beam elements can be used to represent tow sections between crossovers. This approach can simulate the non-orthogonality of two fibre directions; however, interaction properties (e.g. at tow crossovers or resistance to deformation offered by the matrix for prepregs) are usually determined empirically through repeated numerical simulations, with material properties adjusted to provide correlation with experiments[12, 13].

An alternative approach relies on continuum mechanics, where the fabric structure is modelled using one element type[30, 31]. One advantage of this approach is that the constitutive equation developed is not dependent on the element type; also out-of-plane deformation can be simulated. Here, a non-orthogonal constitutive equation is introduced and its applications to forming simulation are discussed. This was developed by Yu *et al.*[30], using a type of homogenisation method to extract macro-material properties by deriving an analytical form for the stress–strain relationship. The constitutive equation consists of two parts: contributions from fibre directional properties and shear properties.

Fibre directional properties

To model the stress and strain relationship dependent on the fibre directional properties, it is important for a constitutive equation to include fibre directions, tow spacing and tow parameters (e.g. fibre diameter). As shown in Fig. 4.6, a structural net comprising several unit cells, one of which is a pair of warp and weft tows with pinned joints, was considered. In modelling of the contribution of fibre directional properties to the constitutive equation, the warp and weft tows are assumed to rotate freely at crossover points. Here, the final form of the equation is presented to explain the difference between the current constitutive form and other forms such as isotropic and orthotropic elastic equations:

$$\begin{bmatrix} \Delta\sigma_{xx} \\ \Delta\sigma_{yy} \\ \Delta\sigma_{xy} \end{bmatrix} = \begin{bmatrix} \frac{\tilde{E}^{\alpha}}{bc} + \Gamma\left(\frac{a}{\bar{h}}\right)\left(\frac{a^2}{c}\right) & \Gamma\left(\frac{a}{\bar{h}}\right)\left(\frac{b^2}{c}\right) & \Gamma\left(\frac{a}{\bar{h}}\right)\left(\frac{ab}{c}\right) \\ \Gamma\left(\frac{b}{\bar{a}}\right)\left(\frac{a^2}{c}\right) & \Gamma\left(\frac{b}{\bar{a}}\right)\left(\frac{b^2}{c}\right) + \frac{\tilde{E}^{\beta}}{\bar{a}c} & \Gamma\left(\frac{b}{\bar{a}}\right)\left(\frac{ab}{c}\right) \\ \Gamma\left(\frac{b}{\bar{h}}\right)\left(\frac{a^2}{c}\right) & \Gamma\left(\frac{b}{\bar{h}}\right)\left(\frac{b^2}{c}\right) & \Gamma\left(\frac{b}{\bar{h}}\right)\left(\frac{ab}{c}\right) \end{bmatrix} \begin{bmatrix} \Delta\varepsilon_{xx} \\ \Delta\varepsilon_{yy} \\ 2\Delta\varepsilon_{xy} \end{bmatrix} \quad 4.2$$

where $a(= |\vec{b}| \cos \Phi)$ and $b\ (= |\vec{b}| \sin \Phi)$ are the projections of the weft tow on the local x- (warp direction) and y-axes respectively, while $\bar{a}\ (= |\vec{a}|)$ and $|\vec{h}|\ (= (b/a)\,\bar{a}\,)$ are the lengths of the warp within a unit cell and the extended height of the weft tow, respectively, as shown in Fig. 4.6 (c = thickness). The

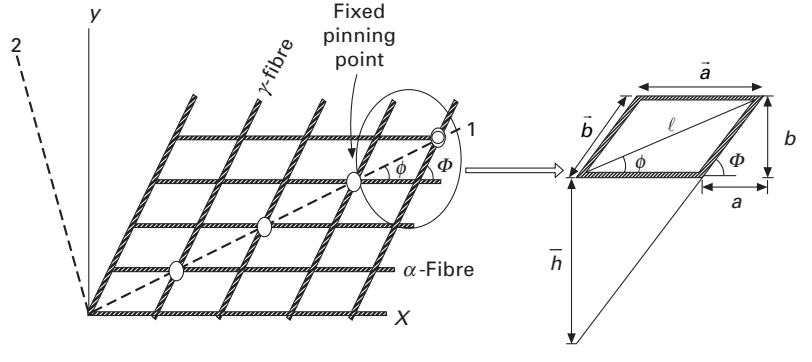

4.6 A structural net (left) and unit cell (right) of a fabric reinforced composite.

two vector quantities, $\vec{a}$ and $\vec{b}$, express the magnitudes and directions of the warp and the weft in a unit cell and define the main internal variables for the constitutive equation. The $\tilde{E}^{\alpha}$ and Γ terms in eqn 4.2 are introduced to represent the stiffness of the warp and the weft tows, and are defined as follows:

$$\tilde{E}^{\alpha} = E^{\alpha}A^{\alpha},\ \Gamma = A^{\gamma}E^{\gamma}/(a^2 + b^2)^{3/2} \qquad 4.3$$

where A^{α} is the cross-sectional area of the warp tow, which is calculated from the number of filaments in the tow and the diameters of the filaments, and E^{α} is the elastic modulus of the fibres, while A^{α} and E^{γ} are the corresponding properties for the weft tow.

Shear properties

Since eqn 4.2 considers only fibre directional properties, a model to incorporate shear stiffness into the constitutive equation is also required. Here, two methods are discussed, one of which utilises a fictitious spring, while another incorporates measured shear properties directly. The former is simple and effective to represent shear stiffness, but it has a drawback in determining the spring constants, which may require repeated numerical simulation, adjusting the spring constants to match the simulation results to the experiment. This idea for treating the inter-tow friction and subsequent locking represents the effect of tow compaction, as the originally orthogonal tows are sheared and hence move closer together (see Fig. 4.7). In eqn 4.2, an additional stiffness term, $\tilde{E}^{\beta}$, can be added to represent the shear stiffness. A full description of this approach is given by Yu *et al.*[30]; a similar approach has been developed recently by Sharma and Sutcliffe[32].

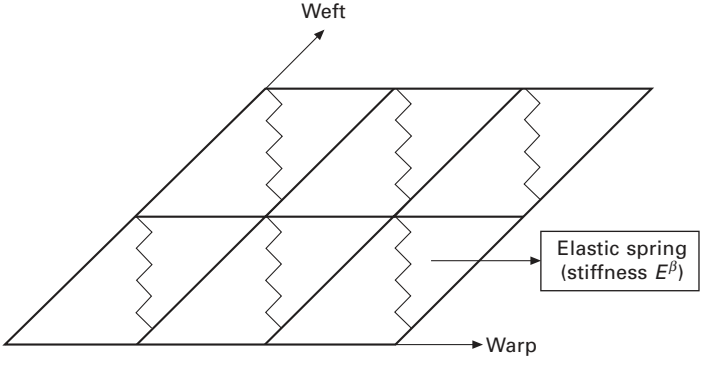

4.7 Scheme for modelling of shear stiffness by a fictitious spring.

An alternative method has been developed, which is rigorous enough to incorporate the material shear force curve directly into the constitutive equation.

The material shear behaviour can be determined either experimentally or analytically as described in Chapters 2 and 3. First, the stresses acting on the non-orthogonal frame are identified during picture frame shear using a covariant basis and the definition of the traction vector. A short description for the shear stiffness model is given in the following section and readers can refer to Yu *et al.*[33, 34] for a detailed derivation.

Consider a square picture frame hinged at each corner as illustrated in Fig. 4.8. The resultant force, $F_R(\gamma)$, is recorded, and this can be converted to the shear force acting on the sides of the frame as follows:

$$F_s = \frac{F_R(\gamma)}{2\cos(\pi/4 - \gamma/2)} \qquad 4.4$$

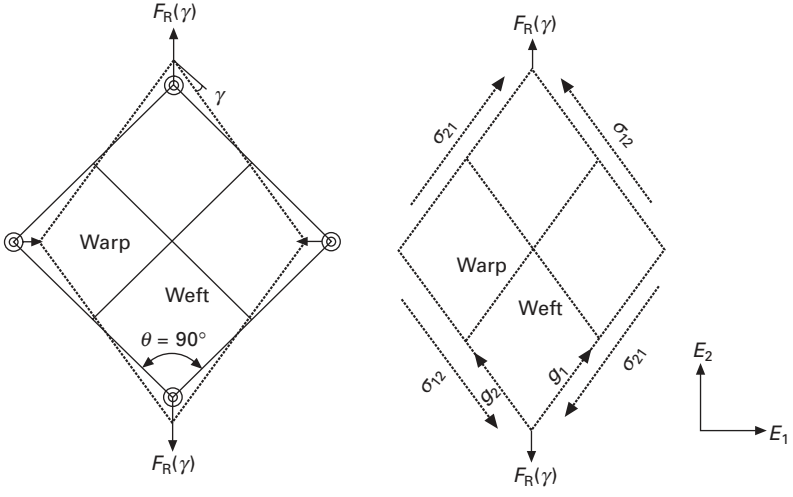

4.8 Schematic of the picture frame shear test (left) and contra-variant stress (σ^{12}, σ^{21}) components acting along normalised covariant base vectors ($\boldsymbol{g}_1$, $\boldsymbol{g}_2$).

On the other hand, during picture frame shear, the actual stresses acting on the specimen can be expressed based on the normalised covariant base vectors ($\boldsymbol{g}_1$ and $\boldsymbol{g}_2$). Note that bold characters represent vector or tensor quantities. The covariant bases (representing two fibre directions), $\boldsymbol{g}_1$ and $\boldsymbol{g}_2$, are unit vectors that may enable two diagonals of the contra-variant metric tensor to be obtained as follows:

$$\boldsymbol{g}_1 = g_1^1 \boldsymbol{E}_1 + g_1^2 \boldsymbol{E}_2, \sqrt{(g_1^1)^2 + (g_1^2)^2} = 1 \qquad 4.5$$

$$\boldsymbol{g}_2 = g_2^1 \boldsymbol{E}_1 + g_2^2 \boldsymbol{E}_2, \sqrt{(g_2^1)^2 + (g_2^2)^2} = 1 \qquad 4.6$$

$$\boldsymbol{g}^{11} = \boldsymbol{g}^1 \cdot \boldsymbol{g}^1 = \frac{1}{\sin^2\theta} = g^{22} = \boldsymbol{g}^2 \cdot \boldsymbol{g}^2 \qquad 4.7$$

where $\boldsymbol{E}_1$ and $\boldsymbol{E}_2$ are inertial bases as shown in Fig. 4.8. Then, the stresses acting on the specimen may be expressed in contra-variant component form from which the tangent stiffness ($\mathrm{d}\boldsymbol{\sigma}/\mathrm{d}\gamma$) due to shear angle increment can be obtained. The stress increment ($\mathrm{d}\boldsymbol{\sigma}$) due to shear angle increment ($\mathrm{d}\gamma$) is then given by:

$$\begin{bmatrix} \Delta\sigma_{xx} \\ \Delta\sigma_{yy} \\ \Delta\sigma_{xy} \end{bmatrix} = \begin{bmatrix} 0 & 0 & 2G_1 g_1^1 g_2^1 + G_2(g_1^1 g_2^2 - g_1^2 g_2^1) \\ 0 & 0 & 2G_1 g_1^2 g_2^2 + G_2(g_1^1 g_2^2 - g_1^2 g_2^1) \\ 0 & 0 & G_1(g_1^1 g_2^2 + g_2^1 g_1^2) \end{bmatrix} \begin{bmatrix} 0 \\ 0 \\ \Delta\gamma \end{bmatrix} \qquad 4.8$$

where

$$G_1 = \frac{1}{lh}\left\{\frac{\mathrm{d}F_s}{\mathrm{d}\gamma}\sqrt{g^{11}} + F_s\sqrt{g^{11}(g^{11}-1)}\right\},\ G_2 = \left(\frac{F_s}{lh}\right)\sqrt{g^{11}} \qquad 4.9$$

in which lh is cross-sectional area of the specimen.

Note that eqn 4.8 is expressed based on a coordinate system that is different from the coordinate system used in the derivation of eqn 4.2. The coordinate system used in eqn 4.2 was constructed based on the warp direction as local x direction, while eqn 4.8 was derived using a coordinate system that bisects the two fibre directions. Therefore, eqn 4.8 needs to be transformed into the coordinate system of eqn 4.1, with the results added to provide the overall constitutive equation.

4.3.3 Application of non-orthogonal constitutive model to forming simulation

To explore the validity of the non-orthogonal equation and its application to composites manufacturing processes, the deformation behaviour of both dry fabric and thermoplastic prepreg are analysed and discussed below.

Stamping simulation for woven dry fabric

This simulation was performed to investigate the forming behaviour of a plain woven fabric using the non-orthogonal constitutive equation. Predicted results were compared with experiments with respect to the boundary profile and fibre angle distribution of the draped preform. An FE model for the draping simulation was constructed as shown in Fig. 4.9 to represent the forming apparatus described by Mohammed *et al.*[35] The radius of the upper mould in this model was 100 mm while that of the lower mould was 97 mm. As the upper mould moved downwards, the fabric was draped over the lower mould, which consisted of a hemispherical dome surrounded by a flat base. The distance from the centre of the lower mould to the edge of the flat base

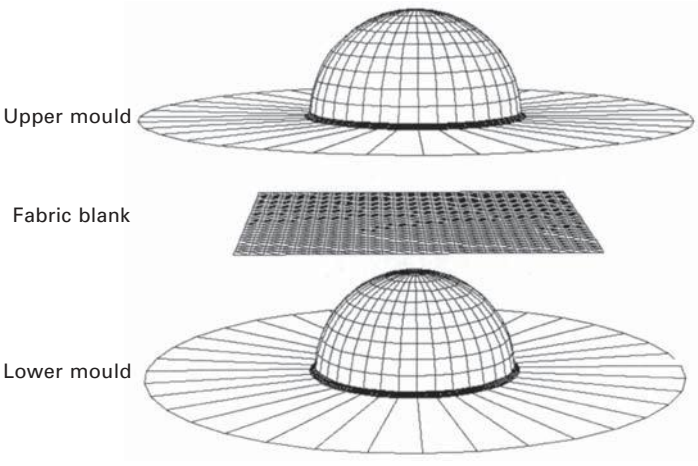

4.9 Finite element model for hemispherical stamping simulation of woven fabric.

was 260 mm. A 320 × 320 mm square of plain woven fabric was used in the experimental study[35]. For the simulation, 1250 triangular shell elements were used to model a quarter section of the woven fabric due to symmetry. The material properties for the fabric blank were calculated based on the structure and material properties of the woven fabric used in the experiment. The friction coefficient between the moulds and the fabric blank was obtained from published data[14]. The material and process variables used in the analysis are listed in Table 4.1. Note that this simulation was performed utilising a spring to represent shear resistance and its stiffness value was tuned to produce good agreement with experimental results.

Table 4.1 Material and structural properties of woven fabric used in draping simulation

	E-glass plain weave
Sheet material	
α fibre stiffness ($\tilde{E}^{\alpha}$)	90 kN
β fibre stiffness ($\tilde{E}^{\gamma}$)	90 kN
Hardening parameter ($\tilde{E}^{\beta}$)	10 N
Structural parameters	
Thickness	0.58 mm
Yarn space	6.25 mm
Friction coefficient	
Upper mould–sheet	0.5
Lower mould–sheet	0.2

Figure 4.10 shows the edge profile of the deformed woven preform. The predicted and measured profiles agree very closely, although there is a little disagreement in the weft direction. This may be due to the assumption that there are no material and structural differences between warp and weft directions in the current simulation.

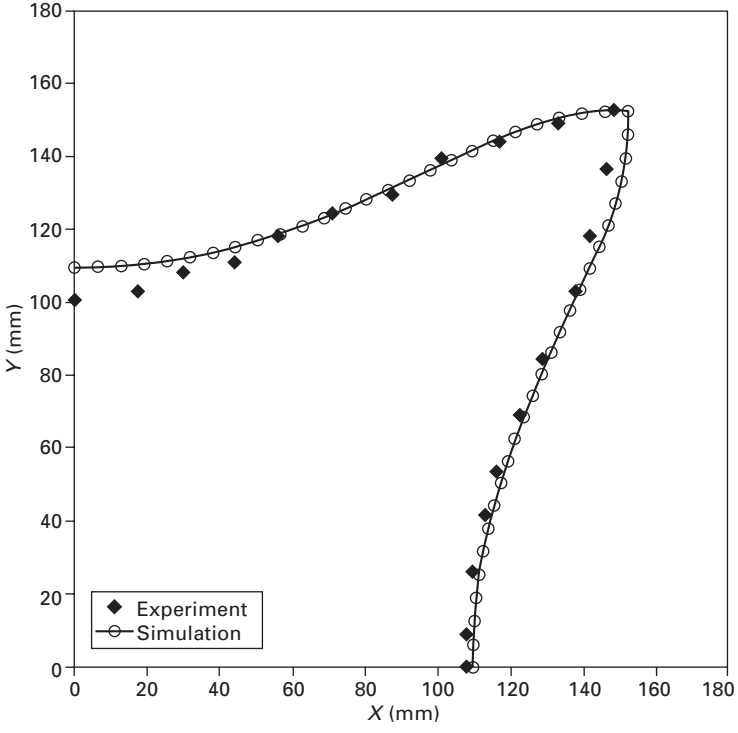

4.10 Comparison between boundary profiles of draped preform from experiment[35] and analysis[30].

Predicted local fibre orientations are represented in Fig. 4.11. Fibre orientation contours were obtained experimentally by measuring the orientation of the deformed gridlines inscribed on the fabric prior to draping[35]. When considering the fibre angle contour for the simulated draped fabric, a region representing 90° inter-fibre angles is observed around the apex of the lower mould, which corresponds to the zero-shear zone. At the equator, where the hemispherical dome changes to the flat surface, the fabric deformation is maximum and an inter-fibre angle of 35.2° was predicted, compared with an experimentally measured fibre angle of 34°. From these comparisons, it can be concluded that the non-orthogonal constitutive equation can simulate the forming behaviour for this material accurately.

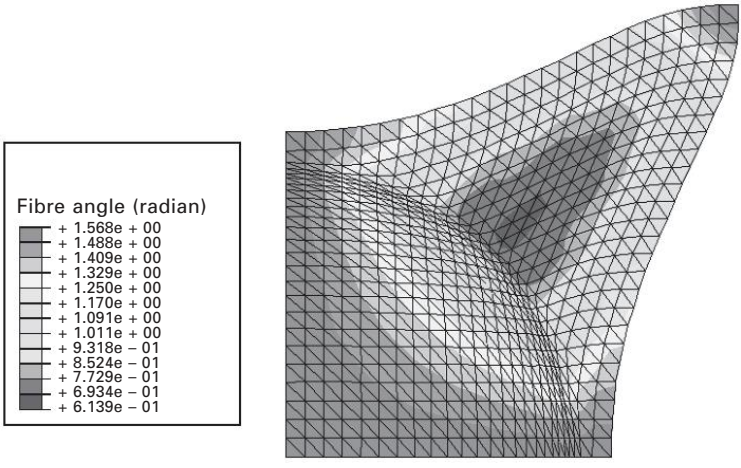

4.11 Predicted fibre angle distribution (radians) for woven fabric hemisphere[30].

Stamping simulation for woven thermoplastic prepreg

The non-orthogonal equation (4.2) can also be applied to thermoplastic prepreg or thermoset prepreg. Here it is assumed that the resin matrix and its interaction with the fibres can be characterised using a picture frame shear test. The deformation behavior of the prepreg is then simulated using eqns 4.2 and 4.8 with the experimental shear data for the prepreg. Rate and temperature effects during forming are ignored in this approach, although Harrison *et al*.[36] have recently implemented a system to account for such effects using a 'look-up table' of material properties, where shear stiffness data are specified as a function of rate and temperature. The alternative is to use a viscous constitutive law directly (see Chapter 3 and de Luca *et al*.[28]), although this is relatively complicated and usually requires model parameters to be determined empirically by comparison between predicted results and specimen tests.

For experimental forming two types of specimens were prepared using a commingled woven fabric: a dry woven fabric with tows comprising commingled glass and polypropylene filaments (as received from the company) and a pre-consolidated plate of the same material (0.5 mm thickness). The consolidated plate was prepared using a 'hot/cold' process in a double compression moulding press with two sets of platens: one hot (205 °C) and the other cold (66 °C). The fabric samples were placed between two polished steel plates, which were then placed into the hot press for approximately 5 mins under 0.344 MPa (50 psi) pressure. Once the matrix had melted, the plates were shuttled to the cold press. Here a larger pressure 1.032 MPa (150 psi) was applied for another 5 mins. For shear property measurement, four layers of commingled woven fabric were consolidated into a laminate, which

was subsequently tested using picture frame shear apparatus[37]. Tests were conducted at the appropriate forming temperature (up to 190 °C) at a constant velocity of 2 mm/s. Typical experimental data for this material are shown in Fig. 4.12.

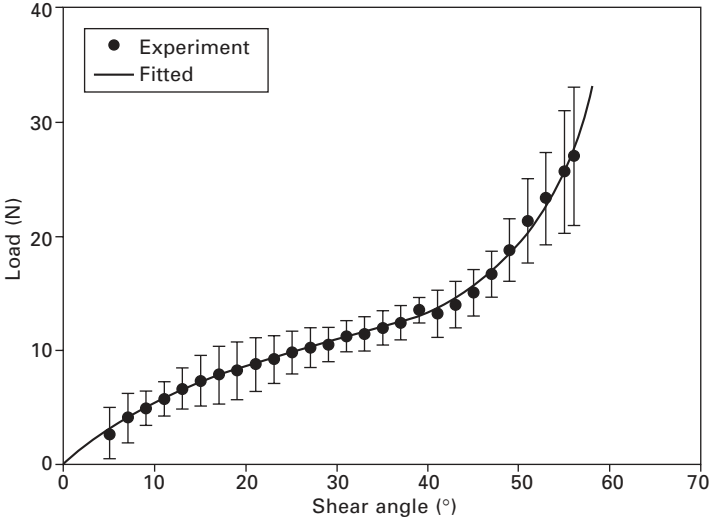

4.12 Averaged experimental load *vs.* shear angle curve during picture-frame shear. Error bar represents the standard deviation of the data from five specimens[37].

The thermoforming press set-up is illustrated in Fig. 4.13. Instead of using a matched female die, the lower chamber was left open to the atmosphere, without any pressure or mould surface used to force the material to take the shape of the punch. To allow the woven thermoplastic blank to draw-in, a 4 mm clearance was maintained between the upper and lower blank-holders. Utilising this set-up specimens were formed and the results were compared against the simulated shapes. The material was drawn to a depth of 0.045 72 m (1.8 inch) using a punch rate of 2 mm/s.

Specimens were formed using both the dry fabric and pre-consolidated materials. The formed shapes showed little difference, despite the fact that the pre-consolidated sheet contained an even distribution of matrix prior to forming whereas the fabric consisted of separate reinforcement and matrix filaments. Fibre angle variations measured along an arc at 45° to the warp direction are shown in Fig. 4.14, in which inter-fibre angle is plotted against arc length from the centre of the specimen.

A circular mesh was constructed using shell elements to simulate stamp forming with the material properties given in Table 4.2. For this simulation using the non-orthogonal constitutive equation, an explicit solver was used

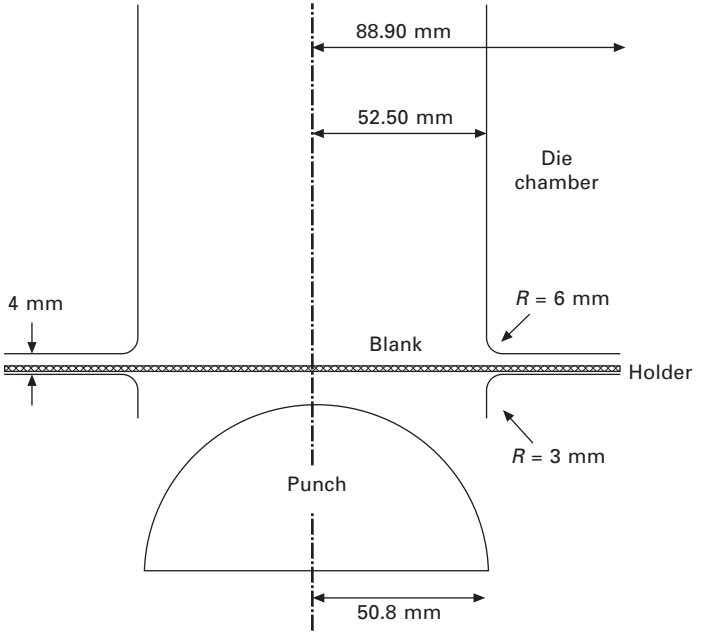

4.13 Thermoforming set-up for woven thermoplastic composites.

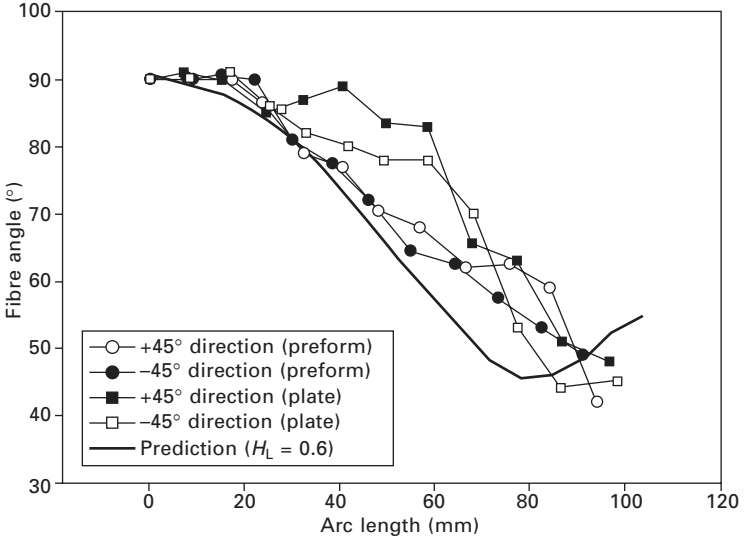

4.14 Inter-fibre angle variations along arc length in ±45° direction for dry commingled fabric (preform) and pre-consolidated (plate) samples[33].

Table 4.2 Structural and material properties of commingled glass–polypropylene plain woven material

Description	Property
Structural parameter	
Elastic modulus of fibres	73 GPa
Yarn spacing	5.25 mm
Plate thickness (1 layer)	0.5 mm
Yarn parameter	
Filaments in warp yarn	1600
Filaments in weft yarn	1600
Filament diameter	18.5 μm

to avoid any divergence problems inherent in the implicit solver due to material non-linearity and contact between the punch and the material. Figure 4.15 shows the stamped shape and fibre angle distribution, which is compared with experimental data in Fig. 4.14. Good agreement was obtained between experimental and simulation results using the non-orthogonal constitutive equation, with the only significant discrepancies around the equator of the hemispherical dome.

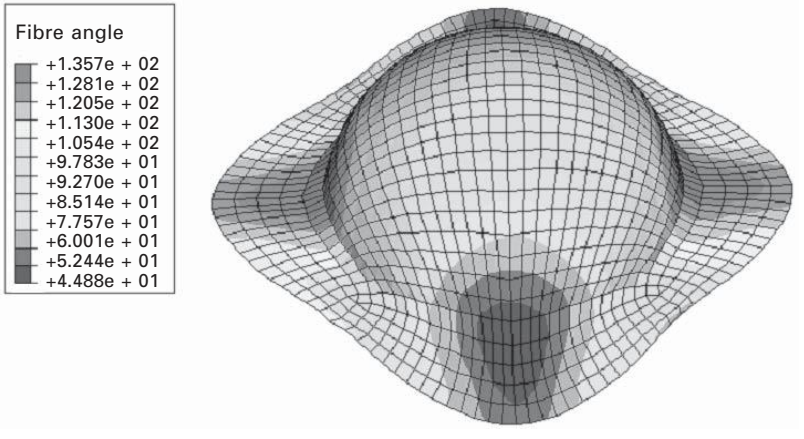

4.15 Formed shape and fibre angle distribution (degrees) predicted using the non-orthogonal constitutive equation and shear material properties[33].

Forming simulation of NCF preform

Studies performed previously at the University of Nottingham[8, 38] have shown that fabric construction can have a significant effect on the shear properties of reinforcements and therefore on their deformed patterns, even for simple shapes such as hemispheres. This is particularly evident for NCFs, in which

reinforcement tows are held together using a warp-knit stitching thread. The stitches in an NCF offer resistance to shearing, so that shearing behaviour in the direction parallel to the stitch can be quite different from that perpendicular to the stitch. This issue was discussed in section 4.2.2, where an iterative mapping approach was used to simulate the forming of NCFs. However, as already noted, this approach does not consider all of the boundary conditions relevant to the forming process. This section models the asymmetric shear behaviour of NCFs using the non-orthogonal constitutive equation, including the shear stiffness model in eqn 4.8. It will focus on whether a continuum mechanics model can simulate the skew symmetric shape of NCF preforms when formed using a hemispherical set-up.

For this example, a ± 45° NCF with a tricot stitch was chosen, and its structural parameters are listed in Table 4.3. The shear behaviour of the NCF was measured by picture frame shear testing[8], and results plotted in Fig. 4.2 show a large difference in shear response according to the shear direction. Non-linear shear force data with respect to shear angle were incorporated into the constitutive equation through eqn 4.8, for which the test results were approximated using non-linear regression. It is not unusual to have some fluctuations in the measured data from picture frame shear testing, particularly at low shear angles. Therefore, the measured data were divided at an arbitrary small shear angle (5°), below which an exponential function was used and above which a polynomial function was used as shown in eqn 4.10. The coefficients for these equations are listed in Table 4.4.

$$\text{if } \gamma < 5°,\ F_s = k_1\gamma + k_2(1 - e^{-k_3\gamma})$$

$$\text{if } \gamma \geq 5°,\ F_s = a_0 + a_1(\gamma - 5) + a_2(\gamma - 5)^2 + a_3(\gamma - 5)^3 + a_4(\gamma - 5)^4 + a_5(\gamma - 5)^5 + a_6(\gamma - 5)^6 \qquad 4.10$$

Table 4.3 Structural and material properties of NCF (COTECH EBX 936)

Description	Property
Structural parameter	
Elastic modulus of fibres	65 GPa
Yarn spacing	0.82 mm
Thickness (assumed)	0.5 mm
Yarn parameter	
Filaments in warp yarn	600
Filaments in weft yarn	600
Filament diameter	16 μm

Next, the shear force data was utilised in the constitutive model to simulate the deformation behaviour of the NCF reinforcement. As a first simulation, the picture frame shear test, which was used to determine the non-linear

Table 4.4 Coefficients for the non-linear curve fitting for NCF shear stiffness parallel and perpendicular to the stitching direction

Coefficients	Parallel	Perpendicular
k_1	1.3639	0.1063
k_2	1.1470	0.9604
k_3	20.9684	6.6138
a_0	7.9670	1.4621
a_1	1.3639	1.0634×10^{-1}
a_2	0.4098	2.8111×10^{-2}
a_3	-4.2656×10^{-2}	-4.1599×10^{-3}
a_4	1.7480×10^{-3}	2.0179×10^{-4}
a_5	-3.2532×10^{-5}	-4.0126×10^{-6}
a_6	2.2958×10^{-7}	2.8625×10^{-8}

shear force curve, was simulated using the same dimensions as the experimental specimen[8]. Membrane finite elements were used to model the picture frame specimen, thus ignoring transverse shear and bending deformations. In this simulation, an implicit solver was utilised. Since the NCF does not show any thickness change during shearing until a large shear angle is reached[8], a constant thickness condition was imposed in this virtual test of picture-frame shear. In Fig. 4.16 predicted load profiles are compared with experimental data, demonstrating good agreement and thus confirming that the shear stiffness model in eqn 4.8 is suitable for simulating NCF shear deformation.

To show the validity of the combined non-orthogonal constitutive equation and shear stiffness model in forming simulation for NCFs, a hemispherical forming process was modelled. The tool for the process consisted of a die, a blank-holder and a punch. The dimension of the punch (radius = 60 mm) was determined based on the forming station at the University of Nottingham[8], while other dimensions were selected to maintain a 2 mm clearance between the punch and the die. Then, an FE model was constructed using triangular elements for the NCF blank and rigid elements for the forming tools, similar to that shown in Fig. 4.9.

An initial study was undertaken to choose the most appropriate element type to represent the fabric. This involved comparison of results obtained using membrane and shell elements. Since the shell element in FE analysis considers a through thickness stress gradient to describe bending behaviour of the material, it involves bending and transverse shear strains in addition to in-plane (membrane) strains. In contrast membrane elements consider only in-plane deformation with no stress gradient through thickness. Hence the use of shell elements requires increased computational time, with analyses here taking three times as long for shell elements than for membrane elements. As the predicted fibre patterns obtained using the two element types were almost identical, membrane elements were used in the present study. However,

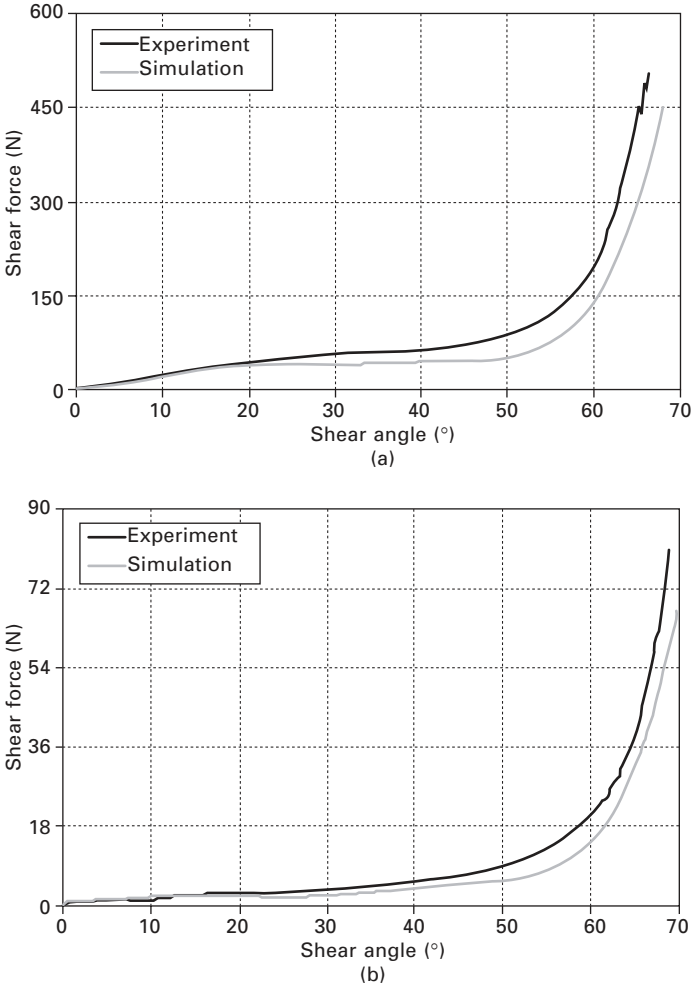

4.16 Comparison of predicted and experimental shear force-shear angle curves. (a) Parallel shear direction and (b) perpendicular shear direction to the stitch in NCF.

shell elements should be considered if the bending behaviour of NCFs is characterised and recognised as an important factor to determine forming behaviour. Furthermore, the shell element is indispensable if spring-forward after forming is considered.

The effect of the blank-holding force (BHF) on the forming behaviour of the NCF was investigated by a parametric study. Here the friction coefficient between the forming tools and the NCF was assumed to be 0.1. BHF values of 0, 1000 and 5000 N (0, 17 421 and 87 105 Pa in pressure) were considered. An increase in BHF is expected to develop tension in the fabric, so that the

formed shape becomes more symmetric as experienced during experiments at Nottingham[8, 38]. This may be possible because high tension applied through the blank-holder suppresses the difference between the shear behaviour according to the positive (parallel to stitch) and the negative (perpendicular to stitch) shear directions. Figure 4.17(a) shows an asymmetric fibre pattern and the possibility of wrinkling when forming is simulated with zero BHF (with only a small blank-holder mass, 650 g, included in the simulation). Figure 4.17(b) shows that the formed shape becomes more symmetric as the BHF increases. This information is useful to design the forming process for a symmetric product, such as a safety helmet, from NCF. In Fig. 4.18, predicted shear angles are compared with experimental measurements[8] along the line of maximum shear on the hemisphere surface, i.e. the bias direction. For the experiments a minimal BHF was used to stop the material from folding during forming. Here the difference in shear angle according to the shear direction was significant, with shear angles in quadrants sheared perpendicular to the stitching thread up to 10° higher than those sheared parallel to the stitch. Predicted shear angles for zero BHF matched experimental values very closely. An increase in BHF is predicted to reduce the shear angle difference between quadrants sheared parallel and perpendicular to the stitch. This is particularly evident at the equator of the hemisphere, where shear deformation is most severe. This matches the trend observed experimentally for other components[8].

A number of simulations were performed to assess the effect of initial blank shape on the formed pattern. In the metal forming field, many research studies were dedicated to the initial blank shape design, with the aim of optimising deformation for a specific product (e.g. Chung and Richmond[39, 40]). The basic idea behind ideal forming starts with the definition of a path that produces a desired homogeneous deformation with minimum plastic work. It is also assumed that formability of local material elements is optimum when they deform according to a minimum work path. An ideal process is then defined as one having local deformations optimally distributed in the final shape, from which the ideal configuration for the initial stage can be determined. Little work has been reported on ideal forming for composite materials. Tucker and coworkers[41, 42] analysed random fibre mats by utilising a forming limit diagram. They determined a potential describing formability that included stretch of the mat and the forming limit, and minimised the potential to seek an ideal initial blank shape where all elements resided within the forming limit. Experimental observations related to the importance of blank shape design were reported by O'Bradaigh[9], who formed several specimens modified from a square blank by progressively removing material from the blank and found that blank shape affected wrinkling behaviour.

To investigate the effect of blank shape on the formed fibre pattern, a forming simulation was performed for a circular blank with a radius of 150

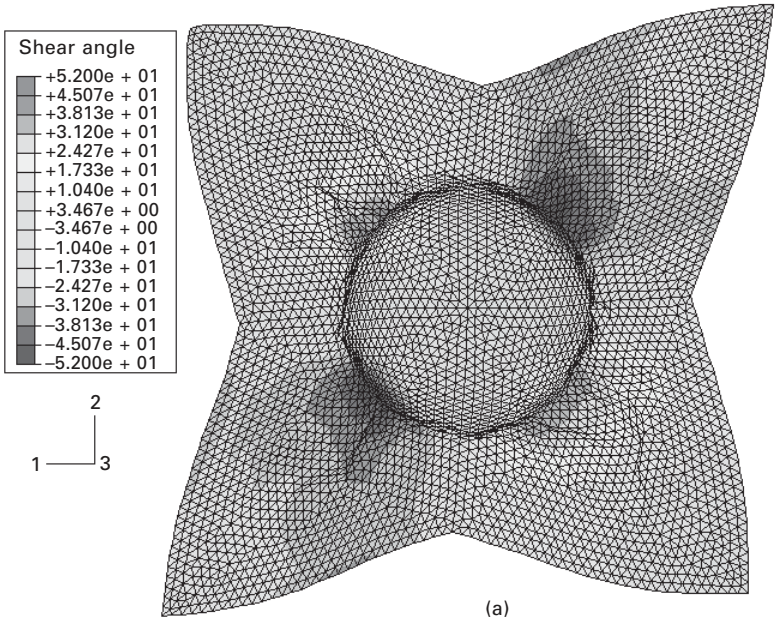

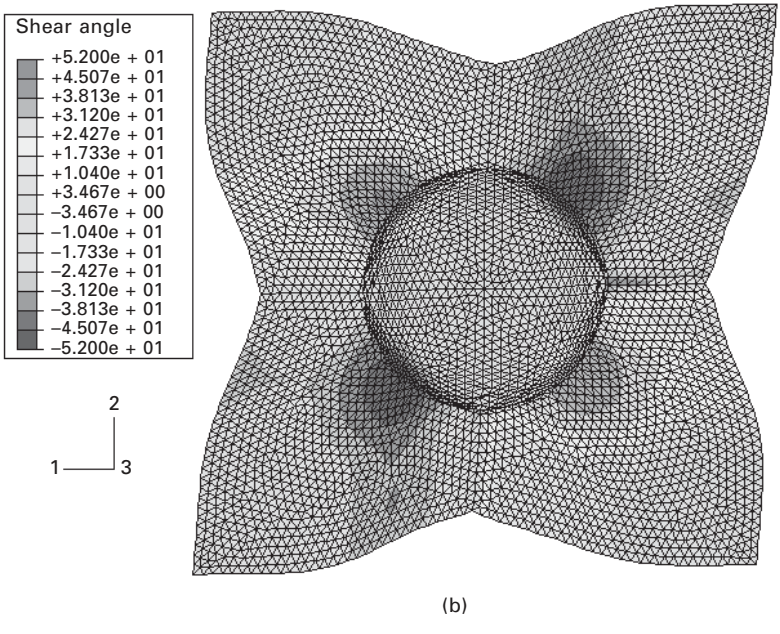

4.17 Effect of blank-holder force (BHF) on the formed shapes: (a) BHF = 0 N; (b) BHF = 5000 N. Shear angles are in degrees.

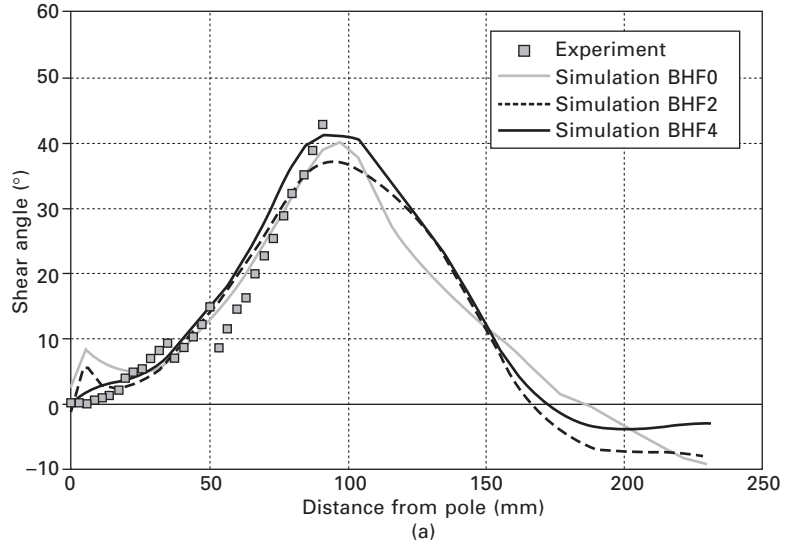

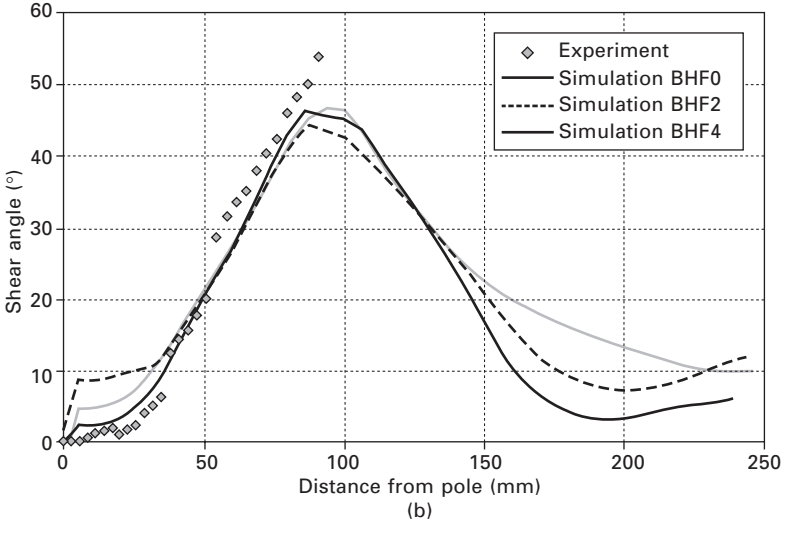

4.18 Comparison between predicted and experimentally measured shear angles for hemisphere formed using an NCF. In the legend BHF0 = 0 N, BHF2 = 1000 N and BHF4 = 5000 N. (a) Quadrant where shear is parallel to the stitching direction. (b) Quadrant where shear is perpendicular to the stitching direction.

mm. The difference between the square and the circular blanks exists in the excess material that lies outside of the blank-holder. The entire edge of the circular blank is initially inside the blank-holder, while the square blank has excess in the bias direction. As the fibres have a high modulus, the edges in

the fibre directions of both the square and circular blanks will be drawn in during forming. Then, they will be kept under the blank-holder throughout the forming process. However, the edges in the bias directions in the square blank, which are extensible via in-plane shearing, will add resistance to forming. This resistance may make shearing in the bias direction difficult, resulting in less shear deformation for the square blank than for the circular blank. As a result the square blank shows a more symmetric formed shape than the circular blank, as shown in Fig. 4.19. This difference is highlighted in Fig. 4.20, which compares the predicted shear angle distributions for both blank shapes. This feature may be advantageous for producing symmetric formed shapes from NCF. More generally this study suggests that blank shape is an important parameter in the design of an optimum forming process for NCF.

4.4 Concluding remarks and future direction

This chapter has presented modelling techniques for forming of bidirectional fabrics and their composites. Kinematic drape models are now relatively mature, and are used widely particularly for hand- lay-up of prepreg. Here the material is modelled as a pin-jointed net, with a geometric approach based on in-plane shear used to map the fabric onto the component surface. This offers a rapid solution, and integration within established CAD/CAM (computer-aided design/manufacture) environments. However the approach is limited in that it cannot represent effects of manufacturing process conditions (e.g. rate, temperature, blank-holder force) or material variables (shear stiffness, tool/ply friction). Some of these limitations are alleviated by modifying the mapping algorithm, using an iterative method where total deformation energy is minimised to select the appropriate mapping. The first step here is to incorporate shear compliance data within the analysis, so that non-symmetric geometries and materials with preferential deformation directions can be modelled. Such an approach was demonstrated in this chapter, and has been shown to provide a more accurate solution than kinematic models for non-crimp fabrics. However there are still limitations here. While current research activities at Nottingham aim to introduce additional energy dissipation terms (e.g. ply-tool friction), a mapping approach is unlikely to represent the physical process accurately, particularly for forming of thermoset or thermoplastic prepregs, where rate and temperature effects may be important. Mapping approaches also only offer a crude approach to predicting wrinkling, via specification of a ‘locking angle’. In practice material wrinkling is a mechanical problem, and occurs in regions subjected to compressive forces beyond the local buckling limit.

The alternative to a mapping approach is to use a mechanical model, where deformation is simulated over a number of time steps. Given an

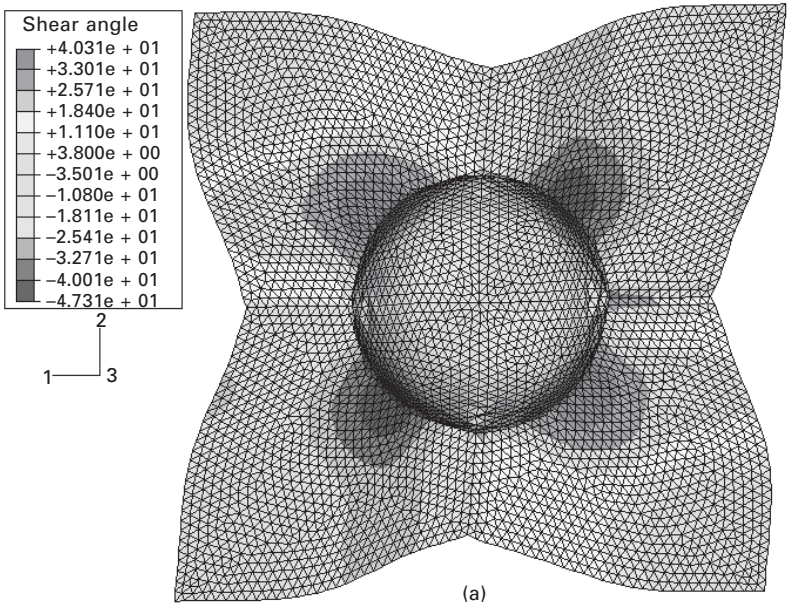

4.19 Effect of blank shape on the formed shape for an NCF hemisphere. (a) Square blank shape (side length = 300 mm). (b) Circular blank shape (diameter = 300 mm). Shear angles are in degrees.

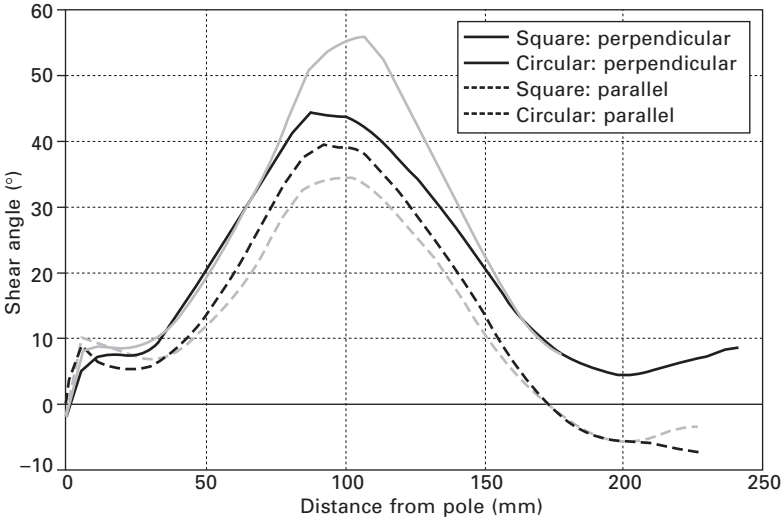

4.20 Predicted shear angle distributions for NCF hemispheres with different blank shapes.

appropriate constitutive model, this approach is able to represent accurate material behaviour and can include realistic boundary conditions. This chapter has focused on one particular model, a non-orthogonal constitutive equation, and its validity and application to forming simulation. Through several simulation examples, forming analyses were performed focusing on three factors: the constitutive equation for the reinforcement, the interface behaviour between the tool and reinforcement, and mechanical processing parameters such as blank-holding force. The model presented here was validated using these examples, and one can conclude that it is reasonably accurate. However, there are numerous published studies on constitutive modelling for forming simulation of continuous fibre reinforced composites. To provide process engineers in industry with an appropriate simulation tool, and to facilitate its utilisation for process design, it is important to recognise both the validity and limitations of a particular constitutive equation. Benchmark simulations for a specified problem would be a good way to compare the many constitutive models available, and an international benchmarking exercise has been initiated recently to address this issue[43].

Since composite sheet forming frequently involves multilayer laminates formed in a single operation, work in this field should be expanded to multilayer analyses by modelling the interface between layers. Two approaches are possible here – either the layers can be modelled separately[28] or a layered element can be used[44] (similar to layered shells used extensively for analysis of laminates). In either case, friction or viscous modelling for the interface is required. Here relatively little data are available, particularly for dry fabrics.

Such data are also required to model automated stamping processes where a blank-holder is used to support the material. Understanding of this type of process is essential if textile-based composites are to progress into high-volume applications.

In this chapter a simulation example was provided to emphasise the importance of blank shape on the deformed fibre pattern for a specific product; this highlights optimisation of blank shape and ideal forming analysis as an important research topic. More generally there is a need for an integrated approach to optimisation in the manufacture of textile composite components. Sheet forming affects several other stages in the manufacturing/performance cycle, for example resin flow in RTM[45, 46] and component mechanical properties[47, 48]. At present each of these stages is analysed in isolation, so that the overall solution may not be optimum. Materials optimisation is also important here, where ideally one should be able to model manufacturing and performance for any combination of polymer and textile without carrying out a long series of characterisation tests. This requires predictive modelling of constitutive behaviour using the approaches discussed in Chapters 2 and 3, and such analyses are now being utilised directly within forming analyses for dry fabric[49] and prepreg[36]. Ultimately such work should result in a general and robust predictive modelling approach for the design and manufacture of textile composite components.

4.5 Acknowledgements

Dr Yu would like to express his gratitude to Dr Farhang Pouboghrat at Michigan State University (USA) and Dr Kwansoo Chung at Seoul National University (Korea), who enthusiastically supported research work on development of the non-orthogonal constitutive equation.

4.6 References

1. Smiley A.J. and Pipes R.B., 'Analysis of the diaphragm forming of continuous fiber reinforced thermoplastics', *J. Thermoplastic Composite Materials*, 1988 **1** 298–321.
2. Van West B.P., Pipes R.B., Keefe M. and Advani S.G., 'The draping and consolidation of comingled fabrics', *Composites Manufacturing*, 1991 **2** 10–22.
3. Bergsma O.K., 'Computer simulation of 3D forming processes of fabric reinforced plastics', *Proc. 9th Int. Conf. on Composite Materials (ICCM-9),* Madrid, 1993, pp. 560–567.
4. Long A.C. and Rudd C.D., 'A simulation of reinforcement deformation during the production of preforms for liquid moulding processes', *Proc. IMechE Part B*, 1994 **208** 269–278.
5. MSC. Patran Laminate Modeler, www.mscsoftware.com
6. FiberSIM 4.0, www.vistagy.com
7. Bunday B.D., *Basic Optimisation Methods*, London, Edward Arnold Ltd, 1984.

8. Souter B.J., Effects of fibre architecture on formability of textile preforms, PhD Thesis, University of Nottingham, 2001.
9. O'Bradaigh C.M., 'Sheet forming of composite materials', in Advani S.G. (ed) *Flow and Rheology in Polymer Composites Manufacturing*, Amsterdam, Elsevier, 1994, 517–569.
10. Krebs J., Friedrich K. and Bhattacharyya D., 'A direct comparison of matched-die versus diaphragm forming', *Composites Part A*, 1998 **29** 183–188.
11. Breen D.E., House D.H. and Wozny M.J., 'A particle-based model for simulating the draping behavior of woven cloth', *Textile Research J.*, 1994 **64**(11) 663–685.
12. Cherouat A. and Billoet J.L., 'Mechanical and numerical modeling of composite manufacturing processes deep-drawing and laying-up of thin pre-impregnated woven fabrics', *J. Materials Processing Technolo.*, 2001 **118**(1–3) 460–471.
13. Sidhu R.M.J.S., Averill R.C., Riaz M. and Pourboghrat F., 'Finite element analysis of textile composite preform stamping', *Composites Structures*, 2001 **52** 483–497.
14. Dong L., Lekakou C. and Bader M.G., 'Solid-mechanics finite element simulations of the draping of fabrics: a sensitivity analysis', *Composites Part A*, 2000 **31** 639–652.
15. O'Bradaigh C.M. and Pipes R.B. 'A finite element formulation for highly anisotropic incompressible elastic solids', *Int. J. Numer. Meth. Eng.*, 1992 **33** 1573–1596.
16. Spencer A.J.M., *Deformations of Fibre Reinforced Materials*, Oxford, Clarendon Press, 1972.
17. Rogers T.G., 'Rheological characterization of anisotropic materials', *Composites*, 1989 **20**(1) 21–27.
18. O'Bradaigh C.M., McGuinness G.B. and Pipes R.B., 'Numerical analysis of stresses and deformations in composite materials sheet forming:central indentation of a circular sheet', *Composites Manufacturing*, 1993 **4**(2) 67–83.
19. Spencer A.J.M., 'Theory of fabric-reinforced viscous fluids', *Composites Part A*, 2000 **31** 1311–1321.
20. Hsiao S.W. and Kikuchi N., 'Numerical analysis and optimal design of composite thermoforming process', *Comput. Methods Appl. Mech. Engrg.*, 1999 **177** 1–34.
21. Takano N., Uetsuji Y., Kahiwagi Y. and Zako M., 'Hierarchical modeling of textile composite materials and structures by the homogenization method', *Modeling Simul. Mater. Sci. Eng.*, 1999 **7** 207–231.
22. Peng X.Q. and Cao J., 'A dual homogenization and finite element approach for material characterization of textile composites', *Composites Part B*, 2002 **33** 45–56.
23. Lim T.C. and Ramakrishna S., 'Modeling of composite sheet forming: a review', *Composites Part A*., 2002 **33** 515–537.
24. ABAQUS FEA software, www.abaqus.com
25. MSC Marc, www.mscsoftware.com
26. ESI PAM-FORM, www.esi-group.com
27. Livermore Software Technology Corporation LS-DYNA, www.dyna3d.com
28. de Luca P., Lefebure P. and Pickett A.K., 'Numerical and experimental investigation of some press forming parameters of two fibre reinforced thermoplastics: APC2-AS4 and PEI-CETEX', *Composites Part A*, 1998 **29** 101–110.
29. Pickett A.K., Queckborner T., de Luca P. and Haug E., 'An explicit finite element solution for the forming prediction of continous fibre-reinforced thermoplastic sheets', *Composites Manufacturing,* 1995 **6**(3–4) 237–243.
30. Yu W.R., Pourboghrat F., Chung K., Zampaloni M. and Kang T.J., 'Non-orthogonal constitutive equation for woven fabric reinforced thermoplastic composites', *Composites Part A*, 2002 **33** 1095–1105.

31. Xue P., Peng X. and Cao J., 'A non-orthogonal constitutive model for characterizing woven composites', *Composites Part A*, 2003 **34** 183–193.
32. Sharma S.B. and Sutcliffe M.P.F., 'A simplified finite element approach to draping of woven fabric', *Proc. 6th Int. ESAFORM Conf. on Material Forming*, Salerno, Italy, Apr 2003, pp. 887–890.
33. Yu W.R., Zampaloni M., Pourboghrat F., Liu L., Chen J., Chung K. and Kang T.J., 'Sheet forming analysis of woven FRT composites using picture-frame shear test and non-orthogonal constitutive equation', *Int. J. Materials and Product Technology*, 2004 **21**(1–3) 71–88.
34. Yu W.R., Harrison P. and Long A.C., 'Forming simulation of non-crimp fabric using non-orthogonal constitutive equation', *Composites Part A*, 2005 **36** 1079–1093.
35. Mohammed U., Lekakou C. and Bader M.G., 'Experimental studies and analysis of the draping of woven fabrics', *Composites Part A*, 2000 **31** 1409–1420.
36. Harrison P., Yu W.R., Long A.C. and Clifford M.J., 'Simulation of viscous textile composite sheet forming based on a unit cell energy model', *Proc. 11th European Conf. on Composite Materials*, Rhodes, Greece, June 2004.
37. Lussier D. and Chen J., 'Material characterization of woven fabrics for thermoforming of composites', *Proc. American Society for Composites 15th Technical Conference*, College Station, Texas, Sept 2000, pp. 301–310.
38. Long A.C., Souter B.J. and Robitaille F., 'Mechanical modelling of in-plane shear and draping for woven and non-crimp reinforcements', *J. Thermoplastic Composite Materials*, 2001 **14** 316–326.
39. Chung K. and Richmond O., 'Ideal forming–I. Homogeneous deformation with minimum plastic work', *Int. J. Mechanical Sci.*, 1992 **34**(7) 575–591.
40. Chung K. and Richmond O., 'Ideal forming-II. Sheet forming with optimum deformation', *Int. J. Mechanical Sci.*, 1992 **34**(8) 617–633.
41. Dessenberger R.B. and Tucker C.L., 'Ideal forming analysis for random fibre preforms', *Transactions of the ASME*, 2003 **125** 146–153.
42. Tucker C.L., 'Forming of advanced composites', in Gutowski T.G. (ed) *Advanced Composite Manufacturing*, New York, John Wiley & Sons, 1997, pp. 297–372.
43. Blanchard P., Cao J., Chen J. and Long A.C. (co-chairs), *NSF workshop on composite sheet forming*, Lowell, M.A., Sept 2001, http://www.mech.northwestern.edu/fac/cao/nsfworkshop/index.htm
44. Lamers E.A.D., Shape distortions in fabric reinforced composite products due to processing induced fibre reorientation, PhD Thesis, University of Twente, 2004.
45. Long A.C., Preform design for liquid moulding processes, PhD Thesis, University of Nottingham, 1994.
46. Bickerton S., Simacek P., Guglielmi S.E. and Advani S.G., 'Investigation of draping and its effect on the mold filling process during manufacturing of a compound curved composite part', *Composites Part A,* 1997 **28A** 801–816.
47. Crookston J., Long A.C. and Jones I.A., 'Modelling effects of reinforcement deformation during manufacturing on elastic properties of textile composites', *Plastics Rubber and Composites*, 2002 **31**(2) 58–65.
48. van den Broucke B., Tuner F., Lomov S.V., Verpoest I., de Luca P. and Dufort L., 'Micro-macro structural analysis of textile composite parts: case study', *Proc. 25th Int. SAMPE Europe Conf.*, Paris, April 2004, pp. 194–199.
49. Boisse P., Daniel J.L. and Soulat D., 'Meso-macro approach for the simulation of textile composite forming', *Proc. 7th Int. Conf. on Textile Composites*, Yamagata, Japan, Sept 2004.